Evaluation of the Sedov-von Neumann-Taylor Blast Wave Solution

James R. Kamm

Integrated Physics Group, MS D413
Applied Physics Division
Los Alamos National Laboratory
Los Alamos, NM 87545 USA

December 21, 2000

LA-UR-00-6055

Contents

List of Figures

List of Tables

Abstract

In this note we state the solution put forward by Sedov [18] for the problem of self-similar, one-dimensional, compressible hydrodynamics in which a finite amount of energy is released at the origin at the initial time. We review the closed-form solution given by Sedov, provde an algorithmic procedure by which this solution can be computed, and compare these results with hydrocode calculations.

1 Introduction

In this note we state the solution put forward by Sedov [18] for the problem of self-similar, one-dimensional, compressible hydrodynamics in which a finite amount of energy is released at the origin at the initial time. This problem is colloquially referred to by some combination of names of the three luminaries that originally obtained the solution to this problem, viz., Sedov [18], Taylor [21], and von Neumann [22]. Of these authors, Sedov provides the most general closed-form solution, which we herein review and compare with hydrocode solutions.

The intention of this note is to distill the thorough exposition given by Sedov into a more compact and accessible form by providing the complete solution together with the procedure by which to compute it. We present the full solution in §2. The reader who desires only to calculate this solution is encouraged to proceed directly to §3, which contains the algorithmic procedure for evaluating the solution. Section 4 contains examples of various solutions as well as comparisons with hydrocode calculations. We close with a summary in §5.

In this report, we identify the corresponding equations of Chapter IV of Sedov's book [18] as an equation number preceded by "S"; e.g., Eq. 1.3 of Chapter IV of [18] is denoted S1.3.

2 The Sedov Solution

In reference [18], Sedov considers the set of equations governing one-dimensional, compressible hydrodynamics. The set of evolution equations governing this behavior is given in physical space as (S1.3)

$$\rho_t + v\,\rho_r + \frac{\rho}{r^{j-1}}\,\left(r^{j-1}\,v\right)_r = 0\,, \tag{1}$$

$$v_t + v\,v_r + \frac{1}{\rho}\,p_r = 0\,, \tag{2}$$

$$(p/\rho^\gamma)_t + u\,(p/\rho^\gamma)_r = 0\,, \tag{3}$$

where ρ is the density, v is the velocity, and p is the pressure. The index $j = 1$, 2, or 3 is the dimensionality index for one-dimensional planar, cylindrical, or

spherical geometry, respectively. Implicit in these equations is the assumption of the polytropic gas equation of state, so that

$$(\gamma - 1)\, e = p/\rho\,, \tag{4}$$

where γ is the constant adiabatic exponent (equal to the ratio of specific heats in this case) and e is the specific internal energy. Additionally, and in distinction to the analysis of Reinicke & Meyer-ter-Vehn [16], heat conduction is assumed to be negligible, so that purely hydrodynamic motion occurs.

The final assumption is that initial density distribution is given by (S14.1)

$$\rho_0(r) = A\, r^{-\omega}\,, \tag{5}$$

where A and ω are constants. When the value of ω is identically zero, the initial density is uniform. Sedov (Ch. IV, §5) shows that the value of ω must be constrained to keep the integral of the density (i.e., the mass) finite according to

$$\omega < j\,. \tag{6}$$

2.1 Similarity Variables

The nondimensionalization of the flow variables is given in S1.1. With the relations preceding S5.12 for the blast wave case, those expressions simplify to the following form:

$$v = \frac{r}{t}\, V\,, \quad \rho = \frac{A}{r^{\omega}}\, R\,, \quad p = \frac{A}{r^{\omega-2}\, t^2}\, P\,, \tag{7}$$

where V, R, and P are the fundamental similarity solution variables. It is a straightforward exercise to show that these quantities are related to other variables according to the following relations (cf. the discussion after S14.4):

$$\frac{r}{r_2} \;\equiv\; \lambda\,, \tag{8}$$

$$\frac{v}{v_2} \;\equiv\; f \equiv \frac{(j+2-\omega)\,(\gamma+1)}{4}\, \lambda\, V\,, \tag{9}$$

$$\frac{\rho}{\rho_2} \;\equiv\; g \equiv \frac{\gamma-1}{\gamma+1}\, \lambda^{-\omega}\, R\,, \tag{10}$$

$$\frac{p}{p_2} \;\equiv\; h \equiv \frac{(j+2-\omega)^2\,(\gamma+1)}{8}\, \lambda^{2-\omega}\, P\,, \tag{11}$$

where the subscript 2 on a variable denotes its immediate post-shock value. In the uniform initial density case ($\omega = 0$), the above relations reduce to the expressions in S11.10. Additionally, the similarity variable Z is defined as (see §2.2 of Ch.4 of [18])

$$Z \equiv \gamma\, P/R\,. \tag{12}$$

An infinitely strong shock is assumed, so that the pre-shock pressure is negligible, i.e., $p_1 \to 0$. This assumption is equivalent to $a_1/U \to 0$, where a_1 is the pre-shock sound speed and U is the shock speed. With this assumption substituted into the standard shock jump relations [23], the immediate post-shock state is determined as:

$$v_2 = \frac{2}{\gamma+1}\,U\,, \quad \rho_2 = \frac{\gamma+1}{\gamma-1}\,\rho_1\,, \quad p_2 = \frac{2}{\gamma+1}\,\rho_1\,U^2\,, \tag{13}$$

where ρ_1 is the immediate pre-shock density.

From dimensional analysis, the shock position $r = r_2$ is related to the total energy $\mathcal{E}_0$ according to the similarity relation (cf. S5.2, S11.3, S14.4)

$$r_2 = \lambda_2 \left(\frac{\mathcal{E}_0}{A\alpha}\right)^{1/(j+2-\omega)} t^{2/(j+2-\omega)}\,. \tag{14}$$

The constant α will be shown (Eq. 66) to be related to the nondimensional energy of the solution. From the above expression, the time t can be written

$$t = r_2^{(j+2-\omega)/2}\,\lambda_2^{-(j+2-\omega)/2}\left(\frac{\mathcal{E}_0}{A\alpha}\right)^{-1/2}\,. \tag{15}$$

Also from Eq. 14, the shock speed $U \equiv dr_2/dt$ can be expressed as (S14.4)

$$\frac{dr_2}{dt} = \frac{2}{j+2-\omega}\,\frac{r_2}{t} = \frac{2}{j+2-\omega}\,r_2^{-(j-\omega)/2}\,\lambda_2^{(j+2-\omega)/2}\left(\frac{\mathcal{E}_0}{A\alpha}\right)^{1/2}\,. \tag{16}$$

2.2 Closed-form Solution

Sedov provides the solution for the constant density initial condition ($\omega = 0$) in all geometries (j = 1,2,3), and for the power law initial density (Eq. 5) in spherical geometry ($j = 3$). Here, we give expressions for the power law initial density valid in in all geometries.

Sedov shows that the unique solution curve passing through the shock point must satisfy the following relation (S14.6)

$$Z = \frac{\gamma-1}{2}\,\frac{V^2\left(V - \frac{2}{j+2-\omega}\right)}{\frac{2}{(j+2-\omega)\,\gamma} - V}\,. \tag{17}$$

There are three possible forms for the solution, all of which satisfy this equation. The correct solution form depends on the relation between the shock state and a singular point of the equations that occurs along the curve given in Eq. 17.

In terms of the similarity variables introduced in the previous section, the shock position r_2 and immediate post-shock state V_2 (S14.5) are given as

$$r = r_2 \;\Leftrightarrow\; \lambda = \lambda_2 = 1 \quad\Leftrightarrow\quad V = V_2 = \frac{4}{(j+2-\omega)\,(\gamma+1)}$$

$$\text{and} \qquad Z = Z_2 = \frac{8\,\gamma\,(\gamma-1)}{(j+2-\omega)^2\,(\gamma+1)^2}\,. \tag{18}$$

There is a singular point of the equations located at (S5.14)

$$V = V^* \;=\; \frac{2}{(\gamma-1)\;j+2}\,, \tag{19}$$

$$Z = Z^* \;=\; \frac{2\,\gamma\,(\gamma-1)\;[(2-\gamma)\,j-\omega]}{[(\gamma-1)\,j+2]^2\,[(\omega-2)\,\gamma-j+2]}\,. \tag{20}$$

For physical solutions that intersect this singular point, it must be true that $Z^* \geq 0$; in this case, it is straightforward to show that ω must satisfy the following constraint (S5.15):

$$\frac{2\gamma+j-2}{\gamma} \geq \omega \geq (2-\gamma)\,j\,, \tag{21}$$

with equality if and only if $Z^* = 0$.

The relation between location of the shock point V_2 and the singular point V^* determines the nature of the solution as follows.

1. $V_2 < V^*$: *Standard*. In this case, a nonzero solution extends from the shock to the origin, at which the pressure is finite. The constraint on the intial density coefficient ω for this case is

$$\omega < \frac{j(3-\gamma)+2(\gamma-1)}{\gamma+1}\,. \tag{22}$$

   The location of the origin corresponds to the values

$$r = 0 \;\Leftrightarrow\; \lambda = \lambda_0 = 0 \;\Leftrightarrow\; V = V_0 = \frac{2}{(j+2-\omega)\;\gamma}\,. \tag{23}$$

   As the origin is approached from the shock, $Z \to +\infty$ and $\lambda \to 0^+$. In this case, the solution space has the domain $V_0 \leq V \leq V_2$.

2. $V_2 = V^*$: *Singular*. In this case, the solution also extends from the shock to the origin, at which the pressure vanishes. This singular case occurs if

$$\omega = \frac{j(3-\gamma)+2(\gamma-1)}{\gamma+1}\,, \tag{24}$$

   in which case the singular point Z^* simplifies to

$$Z^* = \frac{2\,\gamma\,(\gamma-1)}{[(\gamma-1)\;j+2]^2}\,. \tag{25}$$

Alternatively, for a fixed initial density coefficient ω, the singular solution occurs if

$$\gamma = \frac{3j - 2 - \omega}{j - 2 + \omega}\,, \tag{26}$$

from which it is clear that this case cannot occur in a physically realizable planar geometry ($j = 1$) case. In §3, we give a procedure for obtaining the closed-form solution in this case.

3. $V_2 > V^*$: *Vacuum*. In this case, there is a vacuum region of finite dimension centered at the origin. Within the vacuum region, the density vanishes identically, so the values there of, e.g., the pressure and internal energy, are meaningless. A nonzero solution extends from the shock to the vacuum boundary, at which the pressure may be singular. The vacuum case obtains for the following range of initial density coefficients:

$$\omega > \frac{j(3-\gamma) + 2(\gamma - 1)}{\gamma + 1}\,. \tag{27}$$

The location of the vacuum boundary corresponds to the values

$$r = r_v \;\Leftrightarrow\; \lambda = \lambda_v > 0 \;\Leftrightarrow\; V = V_v = \frac{2}{j + 2 - \omega}\,. \tag{28}$$

For a fixed initial density coefficient ω, the vacuum solution occurs according to the following.

(a) In planar geometry ($j = 1$), this case cannot exist for physically realizable configuratons.

(b) In cylindrical geometry ($j = 2$), this case obtains for $\gamma > (4 - \omega)/\omega$ if $0 < \omega < 2$.

(c) In spherical geometry ($j = 3$), this case occurs for $\gamma > (7 - \omega)/(\omega + 1)$ if $-1 < \omega < 3$.

As the vacuum boundary is approached from the shock, $Z \to 0^+$ and $\lambda \to \lambda_v > 0$. In the vacuum case, the nonzero solution space consists of the domain $V_2 \le V \le V_v$.

For the standard and vacuum cases, the closed-form solution can be written by adopting following variables, which depend on the physical parameters j, γ, ω, and the similarity variable V:

$$x_1 \equiv a\,V\,, \tag{29}$$

$$x_2 \equiv b\,(c\,V - 1)\,, \tag{30}$$

$$x_3 \equiv d\,(1 - e\,V)\,, \tag{31}$$

$$x_4 \equiv b\left(1 - \frac{c}{\gamma}\,V\right)\,, \tag{32}$$

where the parameters $a, \ldots, e$ are defined as

$$a \equiv \frac{(j+2-\omega)\,(\gamma+1)}{4}\,, \tag{33}$$

$$b \equiv \frac{\gamma+1}{\gamma-1}\,, \tag{34}$$

$$c \equiv \frac{(j+2-\omega)\,\gamma}{2}\,, \tag{35}$$

$$d \equiv \frac{(j+2-\omega)\,(\gamma+1)}{(j+2-\omega)\,(\gamma+1)-2\,[2+j\,(\gamma-1)]}\,, \tag{36}$$

$$e \equiv \frac{2+j\,(\gamma-1)}{2}\,. \tag{37}$$

Note: The expression for x_3 is indeterminate in the singular case.

In terms of these quantities, the solution given by Sedov (S14.14) assumes the following form:

$$\frac{r}{r_2} \equiv \lambda = x_1^{-\alpha_0}\, x_2^{-\alpha_2}\, x_3^{-\alpha_1}\,, \tag{38}$$

$$\frac{v}{v_2} \equiv f = x_1\,\lambda\,, \tag{39}$$

$$\frac{\rho}{\rho_2} \equiv g = x_1^{\alpha_0\omega}\, x_2^{\alpha_3+\alpha_2\omega}\, x_3^{\alpha_4+\alpha_1\omega}\, x_4^{\alpha_5}\,, \tag{40}$$

$$\frac{p}{p_2} \equiv h = x_1^{\alpha_0 j}\, x_3^{\alpha_4+\alpha_1(\omega-2)}\, x_4^{1+\alpha_5}\,. \tag{41}$$

The α parameters in these expressions are related to the physical parameters as (S14.15):

$$\alpha_0 \equiv \frac{2}{j+2-\omega}\,, \tag{42}$$

$$\alpha_1 \equiv \frac{(j+2-\omega)\,\gamma}{2+j\,(\gamma-1)}\left\{\frac{2\,[j\,(2-\gamma)-\omega]}{\gamma\,(j+2-\omega)^2}-\alpha_2\right\}\,, \tag{43}$$

$$\alpha_2 \equiv -\frac{\gamma-1}{2\,(\gamma-1)+j-\gamma\,\omega}\,, \tag{44}$$

$$\alpha_3 \equiv \frac{j-\omega}{2\,(\gamma-1)+j-\gamma\,\omega}\,, \tag{45}$$

$$\alpha_4 \equiv \frac{(j+2-\omega)\,(j-\omega)}{j\,(2-\gamma)-\omega}\,\alpha_1\,, \tag{46}$$

$$\alpha_5 \equiv \frac{\omega\,(1+\gamma)-2\,j}{j\,(2-\gamma)-\omega}\,. \tag{47}$$

These expressions reduce to Eqs. S11.15 and S11.16 in the uniform initial density ($\omega = 0$) case.

2.3 The Energy Integral

To determine the solution corresponding to a given initial (total) energy released $\mathcal{E}_0$ at the origin, we must relate the solution parameters to that quantity. The energy, which is constant throughout the motion, is the sum of the kinetic and internal energies, which can be expressed in terms of the following integrals:

$$\mathcal{E}_0 = \int_0^{r_s} d\mathcal{V}\,\frac{1}{2}\rho\,v^2 + \int_0^{r_s} d\mathcal{V}\,\frac{p}{\gamma-1}\,, \tag{48}$$

$$= \int_0^{r_s} d\mathcal{V}\,\frac{1}{2}\rho_2\,v_2^2\left(\frac{\gamma-1}{\gamma+1}\,\lambda^{-\omega}\,R\right)\left[\frac{(j+2-\omega)\,(\gamma+1)}{4}\,\lambda\,V\right]^2 + \frac{1}{\gamma-1}\int_0^{r_s} d\mathcal{V}\,p_2\,\frac{(j+2-\omega)^2\,(\gamma+1)}{8}\,\lambda^{2-\omega}\,P\,, \tag{49}$$

where the volume element $d\mathcal{V}$ is defined as

$$d\mathcal{V} \equiv \left(\delta_{j,1} + 2\pi r\delta_{j,2} + 4\pi r^2\delta_{j,3}\right)\,dr\,. \tag{50}$$

For $r_{min} \le r \le r_2$, where

$$r_{min} \equiv \begin{cases} 0, & \text{normal or singular cases} \\ r_v, & \text{vacuum case} \end{cases}\,, \tag{51}$$

we have by definition (Eq. 8) that $r = r_2\,\lambda$ so that $dr = r_2\,d\lambda$, and the volume element becomes

$$d\mathcal{V} = \left(\delta_{j,1} + 2\pi r_2\lambda\,\delta_{j,2} + 4\pi r_2^2\lambda^2\,\delta_{j,3}\right)\,r_2\,d\lambda \tag{52}$$

$$= 2^{j-1}\,r_2^j\,\lambda^{j-1}\,\left(\delta_{j,1} + \pi\delta_{j,2} + \pi\delta_{j,3}\right)\,d\lambda\,. \tag{53}$$

The energy integrals in Eq. 49 vanish in the vacuum region, so, with $r = r_{min}$ corresponding to $\lambda = \lambda_{min}$ and $r = r_2$ corresponding to $\lambda = 1$, the expression in Eq. 49 becomes

$$\mathcal{E}_0 = \int_{\lambda_{min}}^1 d\lambda\;2^{j-1}\,r_2^j\,\lambda^{j-1}\;\left(\delta_{j,1} + \pi\delta_{j,2} + \pi\delta_{j,3}\right) \times \frac{1}{2}\rho_2\,v_2^2\left(\frac{\gamma-1}{\gamma+1}\,\lambda^{-\omega}\,R\right)\left[\frac{(j+2-\omega)\,(\gamma+1)}{4}\,\lambda\,V\right]^2 + \frac{1}{\gamma-1}\int_{\lambda_{min}}^1 d\lambda\;2^{j-1}\,r_2^j\,\lambda^{j-1}\;\left(\delta_{j,1} + \pi\delta_{j,2} + \pi\delta_{j,3}\right) \times p_2\,\frac{(j+2-\omega)^2\,(\gamma+1)}{8}\,\lambda^{2-\omega}\,P\,, \tag{54}$$

$$= (\gamma-1)\;(\gamma+1)\,\frac{(j+2-\omega)^2}{16}\,\rho_2 v_2^2 r_2^j$$

$$\times\ 2^{j-2}\ (\delta_{j,1}+\pi\delta_{j,2}+\pi\delta_{j,3})\int_{\lambda_{min}}^{1} d\lambda\ \lambda^{j+1-\omega}RV^2$$

$$+\ \frac{(j+2-\omega)^2\,(\gamma+1)}{8}\,p_2 r_2^j$$

$$\times\ \frac{2^{j-1}}{\gamma-1}\,(\delta_{j,1}+\pi\delta_{j,2}+\pi\delta_{j,3})\int_{\lambda_{min}}^{1} d\lambda\ \lambda^{j+1-\omega}P\,, \tag{55}$$

$$= (\gamma-1)(\gamma+1)\,\frac{(j+2-\omega)^2}{16}\,\rho_2 v_2^2 r_2^j\,I_1+\frac{(j+2-\omega)^2(\gamma+1)}{8}\,p_2 r_2^j I_2\,, \tag{56}$$

where

$$I_1 \equiv 2^{j-2}\ (\delta_{j,1}+\pi\delta_{j,2}+\pi\delta_{j,3})\ J_1 \quad \text{and} \tag{57}$$

$$I_2 \equiv \frac{2^{j-1}}{\gamma-1}\,(\delta_{j,1}+\pi\delta_{j,2}+\pi\delta_{j,3})\ J_2\,, \tag{58}$$

with J_1 and J_2 defined as

$$J_1 \equiv \int_{\lambda_{min}}^{1} d\lambda\ \lambda^{j+1-\omega}RV^2 \quad \text{and} \quad J_2 \equiv \int_{\lambda_{min}}^{1} d\lambda\ \lambda^{j+1-\omega}P\,. \tag{59}$$

To evaluate Eq. 56 for the total energy, we require expressions for the immediate post-shock state (Eq. 13). The value of the immediate pre-shock density ρ_1 is obtained from Eq. 5 using the expression in Eq. 14 for the shock position (with $\lambda_2 = 1$):

$$\rho_1 = A\,r_2^{-\omega} = A\left(\frac{\mathcal{E}_0}{A\,\alpha}\right)^{-\omega/(j+2-\omega)} t^{-2\,\omega/(j+2-\omega)}\,. \tag{60}$$

From this expression and Eq. 16 for the shock speed, the immediate post-shock values may be expressed as

$$v_2 = \frac{4}{(\gamma+1)\,(j+2-\omega)}\left(\frac{\mathcal{E}_0}{A\,\alpha}\right)^{1/(j+2-\omega)} t^{(\omega-j)/(j+2-\omega)}\,, \tag{61}$$

$$\rho_2 = \frac{\gamma+1}{\gamma-1}\,A\,\left(\frac{\mathcal{E}_0}{A\,\alpha}\right)^{-\omega/(j+2-\omega)} t^{(-2\,\omega)/(j+2-\omega)}\,, \tag{62}$$

$$p_2 = \frac{8}{(\gamma+1)\,(j+2-\omega)^2}\,A\,\left(\frac{\mathcal{E}_0}{A\,\alpha}\right)^{(2-\omega)/(j+2-\omega)} t^{-2j/(j+2-\omega)}\,. \tag{63}$$

Substituting these values into Eq. 56 for the total enegy, the following simplification obtains:

$$\mathcal{E}_0 = (\gamma-1)\ (\gamma+1)\,\frac{(j+2-\omega)^2}{16}\,\frac{\gamma+1}{\gamma-1}\,A\left(\frac{\mathcal{E}_0}{A\,\alpha}\right)^{-\omega/(j+2-\omega)} t^{-2\,\omega/(j+2-\omega)}$$

$$\times \left[\frac{4}{(\gamma+1)\,(j+2-\omega)} \left(\frac{\mathcal{E}_0}{A\,\alpha} \right)^{1/(j+2-\omega)} t^{(\omega-j)/(j+2-\omega)} \right]^2$$

$$\times \left(\frac{\mathcal{E}_0}{A\,\alpha} \right)^{j/(j+2-\omega)} t^{2j/(j+2-\omega)}\, I_1$$

$$+ \frac{(j+2-\omega)^2\,(\gamma+1)}{8} \frac{8}{(\gamma+1)\,(j+2-\omega)^2}\, A \left(\frac{\mathcal{E}_0}{A\,\alpha} \right)^{(2-\omega)/(j+2-\omega)}$$

$$\times\, t^{-2j/(j+2-\omega)} \left(\frac{\mathcal{E}_0}{A\,\alpha} \right)^{j/(j+2-\omega))} t^{2j/(j+2-\omega)}\, I_2\,, \tag{64}$$

$$= A \left(\frac{\mathcal{E}_0}{A\,\alpha} \right)^{(-\omega+2+j)/(j+2-\omega)} t^{(-2\omega+2\omega-2j+2j)/(j+2-\omega)}\, I_1$$

$$+ A \left(\frac{\mathcal{E}_0}{A\,\alpha} \right)^{(2-\omega+j)/(j+2-\omega)} t^{(-2j+2j)/(j+2-\omega)}\, I_2\,, \tag{65}$$

$$\Rightarrow\ \mathcal{E}_0 = A \left(\frac{\mathcal{E}_0}{A\,\alpha} \right) (I_1 + I_2) \quad \Rightarrow \quad \alpha = I_1 + I_2\,. \tag{66}$$

Thus, the constant α is the sum of the two integrals, given in Eqs. 57–59.

2.3.1 Standard or Vacuum Case

In either the standard ($V_2 < V^*$) or vacuum ($V_2 > V^*$) case, one can evaluate the integrals J_1 and J_2 by performing a change of variables from λ to V:

$$J_1 = \int_{\lambda_{min}}^{1} d\lambda\ \lambda^{j+1-\omega} R V^2 = \int_{V_{min}}^{V_2} dV\, \frac{d\lambda}{dV} \lambda(V)^{j+1-\omega} R(V) V^2\,, \tag{67}$$

$$J_2 = \int_{\lambda_{min}}^{1} d\lambda\ \lambda^{j+1-\omega} P = \int_{V_{min}}^{V_2} dV\, \frac{d\lambda}{dV} \lambda(V)^{j+1-\omega} P(V)\,, \tag{68}$$

where V_{min} is either V_0 (Eq. 23) or V_v (Eq. 28), and V_2 is given in Eq. 18. We simplify the integrands in these expressions prior to evaluating them numerically. The expression for λ in Eq. 38 can be written in the form

$$\lambda(V) = [aV]^{-\alpha_0}\ [b\,(cV-1)]^{-\alpha_2}\ [d\,(1-eV)]^{-\alpha_1}\ , \tag{69}$$

where the various constants $a, \ldots, e$ are given in Eqs. 33–37. Taking the logarithmic derivative of this quantity yields

$$\frac{d\lambda}{dV} = -\left[\frac{\alpha_0}{V} + \frac{\alpha_2 c}{cV-1} - \frac{\alpha_1 e}{1-eV} \right] \lambda(V)\,, \tag{70}$$

which can be evaluated explicitly as a function of V.

The expression for $R(V)$ is derived from Eqs. 10 and 40. These relations imply that

$$\lambda^{-\omega}\, R(V) = \frac{\gamma+1}{\gamma-1}\, g = \frac{\gamma+1}{\gamma-1}\, [aV]^{\alpha_0\omega}\, [b\,(cV-1)]^{\alpha_3+\alpha_2\omega} \times \left[d\,(1-eV)\right]^{\alpha_4+\alpha_1\omega} \left[b\left(1-\frac{c}{\gamma}V\right)\right]^{\alpha_5}. \quad (71)$$

Similarly, the expression for $P(V)$ is derived from Eqs. 12, 17, and 35, which together imply that

$$\lambda^{-\omega}\, P(V) = \frac{1}{\gamma}\, \lambda^{-\omega}\, R\, Z = \frac{1}{\gamma}\, \frac{\gamma+1}{\gamma-1}\, [aV]^{\alpha_0\omega}\, [b\,(cV-1)]^{\alpha_3+\alpha_2\omega} \times \left[d\,(1-eV)\right]^{\alpha_4+\alpha_1\omega} \left[b\left(1-\frac{c}{\gamma}V\right)\right]^{\alpha_5} \quad \frac{(\gamma-1)\, V^2\, (cV-\gamma)}{2\,(1-cV)}. \quad (72)$$

Using these relations, explicit expressions for the integrands of J_1 and J_2 can be obtained in terms of the similarity variable V. Specifically, the integrand of J_1 can be simplified to the following expression:

$$\begin{aligned}\frac{d\lambda}{dV}\, \lambda^{j+1}\, \left(\lambda^{-\omega}R\right)\, V^2 \;&=\; -\frac{\gamma+1}{\gamma-1}\, V^2 \left[\frac{\alpha_0}{V} + \frac{\alpha_2 c}{cV-1} - \frac{\alpha_1 e}{1-eV}\right] [aV]^{-(j+2-\omega)\alpha_0} \\ &\times [b\,(cV-1)]^{-(j+2-\omega)\alpha_2+\alpha_3}\, [d\,(1-eV)]^{-(j+2-\omega)\alpha_1+\alpha_4} \left[b\left(1-\frac{c}{\gamma}V\right)\right]^{\alpha_5} \\ &=\; -\frac{\gamma+1}{\gamma-1}\, V^2 \left[\frac{\alpha_0}{V} + \frac{\alpha_2 c}{cV-1} - \frac{\alpha_1 e}{1-eV}\right] \\ &\times \left\{[aV]^{\alpha_0}\, [b\,(cV-1)]^{\alpha_2}\, [d\,(1-eV)]^{\alpha_1}\right\}^{-(j+2-\omega)} \\ &\times [b\,(cV-1)]^{\alpha_3}\, [d\,(1-eV)]^{\alpha_4} \left[b\left(1-\frac{c}{\gamma}V\right)\right]^{\alpha_5}. \end{aligned} \quad (73)$$

Similarly, the integrand of J_2 can be written as follows:

$$\begin{aligned}\frac{d\lambda}{dV}\, \lambda^{j+1}\, \left(\lambda^{-\omega}P\right) \;&=\; -\frac{\gamma+1}{2\gamma}\, V^2 \left(\frac{cV-\gamma}{1-cV}\right) \left[\frac{\alpha_0}{V} + \frac{\alpha_2 c}{cV-1} - \frac{\alpha_1 e}{1-eV}\right] \\ &\times \left\{[aV]^{\alpha_0}\, [b\,(cV-1)]^{\alpha_2}\, [d\,(1-eV)]^{\alpha_1}\right\}^{-(j+2-\omega)} \\ &\times [b\,(cV-1)]^{\alpha_3}\, [d\,(1-eV)]^{\alpha_4} \left[b\left(1-\frac{c}{\gamma}V\right)\right]^{\alpha_5}. \end{aligned} \quad (74)$$

It is these functions that are used in numerical quadrature routines (ACM algorithm 691 [24]) to evaulate J_1 and J_2.

2.3.2 Singular Case

In the singular case ($V_2 = V^*$), the integrals J_1 and J_2 can be evaluated explicitly. Recall that the physically realizable (i.e., finite mass) singular case can occur only in cylindrical or spherical geometries, so that $j \neq 1$, and that the range of λ is $[0, 1]$. We first obtain simplified expressions for the similarity variables R and P, then evaluate the integrals.

In the singular case, Eq. S2.3 for the equation governing R reduces to

$$\left(V^* - \frac{2}{2+j-\omega}\right) \frac{d\,(\log R)}{d\,(\log \lambda)} = (\omega - j)\, V^* \,. \tag{75}$$

It is a straightforward exercise to show that the solution to this equation is

$$R = B\, \lambda^{4(j-1)/(\gamma+1)} \,, \tag{76}$$

where B is a constant and we have used Eqs. 19 for V^* and 24 for ω in the simplification. From Eq. 10,

$$\rho = \rho_2 \frac{\gamma-1}{\gamma+1} \lambda^{-\omega} R = \rho_2 \frac{\gamma-1}{\gamma+1} B\, \lambda^{-\omega+[\,4(j-1)/(\gamma+1)\,]} \,. \tag{77}$$

Evaluating this at the immediate post-shock state ($\lambda = 1$), we find that

$$\rho_2 = B\, \rho_2 \frac{\gamma-1}{\gamma+1} \quad \Rightarrow \quad B = \frac{\gamma+1}{\gamma-1} \quad \Rightarrow \quad R = \frac{\gamma+1}{\gamma-1} \lambda^{4(j-1)/(\gamma+1)} \,. \tag{78}$$

The similarity variable P is given in terms of R and Z in Eq. 12. Using that relation together with the above solution for R and Eq. 25 for Z^*, the following expression for P obtains:

$$P = \frac{2\,(\gamma+1)}{[(\gamma-1)\,j+2]^2} \lambda^{4(j-1)/(\gamma+1)} \,. \tag{79}$$

Using these results, we can evaluate J_1 and J_2. Upon substituting these expressions into Eq. 59 and using Eq. 24 for ω, we obtain:

$$\begin{aligned}
J_1 &= \int_0^1 d\lambda\; \lambda^{j+1-\omega}\, R\, V^2 \\
&= (V^*)^2\; \frac{\gamma+1}{\gamma-1} \int_0^1 d\lambda\; \lambda^{\frac{4(j-1)}{(\gamma+1)} + \frac{(j+1)\cdot(\gamma+1)}{(\gamma+1)} - \frac{j(3-\gamma)+2(\gamma-1)}{(\gamma+1)}} \,, \\
&= \left[\frac{2}{(\gamma-1)j+2}\right]^2 \frac{\gamma+1}{\gamma-1} \int_0^1 d\lambda\; \lambda^{(4j-4+j+\gamma j+\gamma+1-3j+\gamma j-2\gamma+2)/(\gamma+1)} \,, \\
&= \left[\frac{2}{(\gamma-1)j+2}\right]^2 \frac{\gamma+1}{\gamma-1} \int_0^1 d\lambda\; \lambda^{(2j+2\gamma j-\gamma-1)/(\gamma+1)} \,,
\end{aligned}$$

$$
\begin{aligned}
&= \left[\frac{2}{(\gamma-1)j+2}\right]^2 \frac{\gamma+1}{\gamma-1} \int_0^1 d\lambda\ \lambda^{[2j(\gamma+1)-(\gamma+1)]/(\gamma+1)}\,, \\
&= \left[\frac{2}{(\gamma-1)j+2}\right]^2 \frac{\gamma+1}{\gamma-1} \int_0^1 d\lambda\ \lambda^{2j-1}\,, \\
&= \left[\frac{2}{(\gamma-1)j+2}\right]^2 \frac{\gamma+1}{\gamma-1} \frac{\lambda^{2j}}{2j}\Bigg|_0^1, \\
\Rightarrow\quad J_1 &= \frac{\gamma+1}{\gamma-1} \frac{2}{j\ [(\gamma-1)j+2]^2}\,. \qquad (80)
\end{aligned}
$$

and

$$
\begin{aligned}
J_2 &= \int_0^1 d\lambda\ \lambda^{j+1-\omega}\, P \\
&= \frac{2\ (\gamma+1)}{[(\gamma-1)\,j+2]^2} \int_0^1 d\lambda\ \lambda^{\frac{4(j-1)}{(\gamma+1)}+\frac{(j+1)\cdot(\gamma+1)}{(\gamma+1)}-\frac{j(3-\gamma)+2(\gamma-1)}{(\gamma+1)}} \\
&= \frac{2\ (\gamma+1)}{[(\gamma-1)\,j+2]^2} \int_0^1 d\lambda\ \lambda^{2j-1} \\
&= \frac{2\ (\gamma+1)}{[(\gamma-1)+2]^2} \frac{\lambda^{2j}}{2j}\Bigg|_0^1 \\
\Rightarrow\quad J_2 &= \frac{\gamma+1}{j\ [(\gamma-1)+2]^2}\,. \qquad (81)
\end{aligned}
$$

Using these expressions we evaluate I_1 (Eq. 57) and I_2 (Eq. 58):

$$
\begin{aligned}
I_1 &= 2^{j-2}\ (\delta_{j,1}+\pi\delta_{j,2}+\pi\delta_{j,3})\ \frac{\gamma+1}{\gamma-1}\ \frac{2}{j\ [(\gamma-1)j+2]^2}\,, \\
&= \frac{\gamma+1}{\gamma-1}\ (\delta_{j,1}+\pi\delta_{j,2}+\pi\delta_{j,3})\ \frac{2^{j-1}}{j\ [(\gamma-1)\,j+2]^2} \quad \text{and} \qquad (82) \\
I_2 &= \frac{2^{j-1}}{\gamma-1}\,(\delta_{j,1}+\pi\delta_{j,2}+\pi\delta_{j,3})\ \frac{\gamma+1}{j\ [(\gamma-1)+2]^2}\,, \\
&= \frac{\gamma+1}{\gamma-1}\ (\delta_{j,1}+\pi\delta_{j,2}+\pi\delta_{j,3})\ \frac{2^{j-1}}{j\ [(\gamma-1)\,j+2]^2}\,, \qquad (83) \\
\Rightarrow I_1 &= I_2\,. \qquad (84)
\end{aligned}
$$

Using these results, a closed-form expression for the constant α (Eq. 66) obtains:

$$
\alpha = \frac{\gamma+1}{\gamma-1}\ (\delta_{j,1}+\pi\delta_{j,2}+\pi\delta_{j,3})\ \frac{2^j}{j\ [(\gamma-1)\,j+2]^2}\,. \qquad (85)
$$

Further simplifications obtain in the singular case. Since V is constant (Eq. 19) and the closed-form expressions for both R and P are known (Eqs. 78 and 79), the expressions given in Eq. 7 for the physical variables can be written

$$v = \frac{r}{t}\,V^*,\ \rho = \frac{A}{r^\omega}\,\frac{\gamma+1}{\gamma-1}\,\lambda^{4(j-1)/(\gamma+1)},\ p = \frac{A}{r^{\omega-2}\,t^2}\,\frac{2\,(\gamma+1)}{\left[(\gamma-1)\,j+2\right]^2}\,\lambda^{4(j-1)/(\gamma+1)}\,. \tag{86}$$

We evaluate each of these expressions at the immediate post-shock state, and use those results to obtain simplified expressions for these quantities.

For the velocity,

$$v_2 = \frac{r_2}{t}\,V^* \quad \Rightarrow \quad V^* = \frac{t v_2}{r_2}\,. \tag{87}$$

Substituting this result into the expression for v in Eq. 86 and using the expression for λ in Eq. 8, we find that

$$\begin{aligned} \frac{v}{v_2} &= \frac{r}{t}\,V^* \times \frac{t}{r_2}\,\frac{1}{V^*} = \frac{r}{r_2} \\ \Rightarrow \quad \frac{v}{v_2} &= \lambda\,. \end{aligned} \tag{88}$$

For the density, the post-shock state is

$$\rho_2 = \frac{A}{r_2^\omega}\,\frac{\gamma+1}{\gamma-1} \tag{89}$$

so that

$$\begin{aligned} \frac{\rho}{\rho_2} &= \frac{A}{r^\omega}\,\frac{\gamma+1}{\gamma-1}\,\lambda^{4(j-1)/(\gamma+1)} \times \frac{r_2^\omega}{A}\,\frac{\gamma-1}{\gamma+1}\,, \\ &= \left(\frac{r}{r_2}\right)^{-\omega}\,\lambda^{4(j-1)/(\gamma+1)} = \lambda^{\frac{4(j-1)}{\gamma+1}-\omega}\,, \\ &= \lambda^{\frac{4j-4-3j+j\gamma-2\gamma+2}{\gamma+1}} = \lambda^{\frac{j+j\gamma-2\gamma-2}{\gamma+1}} = \lambda^{\frac{j(\gamma+1)-2(\gamma+1)}{\gamma+1}}\,, \\ \Rightarrow \quad \frac{\rho}{\rho_2} &= \lambda^{j-2}\,, \end{aligned} \tag{90}$$

where we have used Eq. 24 for ω.

For the pressure, the post-shock state is

$$p_2 = \frac{A}{r_2^\omega}\,\left(\frac{r_2}{t}\right)^2\,\frac{2\,(\gamma+1)}{\left[(\gamma-1)\,j+2\right]^2}\,. \tag{91}$$

This result implies that

$$\begin{aligned} \frac{p}{p_2} &= \frac{A}{r^\omega}\left(\frac{r}{t}\right)^2\frac{2\,(\gamma+1)}{\left[(\gamma-1)\,j+2\right]^2}\,\lambda^{4(j-1)/(\gamma+1)} \times \frac{r_2^\omega}{A}\left(\frac{t}{r_2}\right)^2\frac{\left[(\gamma-1)\,j+2\right]^2}{2\,(\gamma+1)} \\ &= \left(\frac{r}{r_2}\right)^{2-\omega}\lambda^{4(j-1)/(\gamma+1)} = \lambda^{\frac{4(j-1)}{\gamma+1}-\omega+2}\,, \\ \Rightarrow \quad \frac{p}{p_2} &= \lambda^j\,. \end{aligned} \tag{92}$$

Using Eqs. 4, 90, and 92, it is a straightforward exercise to show that the SIE in the singular case varies quadratically with λ as

$$\frac{e}{e_2} = \lambda^2 \,. \tag{93}$$

3 Numerical Evaluation of the Sedov Solution

In this section we describe how to numerically evaluate the solution to the Sedov problem, given the prescribed initial parameters and the expressions presented above. The numerical evaluation of the solution proceeds in a manner inverse to the previous exposition. The following is a step-by-step method by which to evaluate the solution for a given energy $\mathcal{E}_0$.

1. Evaluate the similiarity shock position V_2 (Eq. 18) and the similarity singular point V^* (Eq. 19).

2. Evaluate the energy integrals by calculating α as follows:

   (a) If either $V_2 < V^*$ (*standard*) or $V_2 > V^*$ (*vacuum*), then:

      i. Numerically evaluate the integral J_1 according to Eq. 67 using the expression for the integrand in Eq. 73.

      ii. Numerically evaluate the integral J_2 according to Eq. 68 using the expression for the integrand in Eq. 74.

      iii. Using J_1 and J_2, calculate $\alpha = I_1 + I_2$ using Eqs. 57 and 58.

   (b) Else $V_2 = V^*$ (*singular*), so:

      i. Evaluate α explicitly using Eq. 85.

3. At each time $t > 0$, evaluate the following in the given order.

   (a) The shock position (Eq. 14): $r_2 = [\mathcal{E}_0/(\alpha\, A)]^{1/(j+2-\omega)}\; t^{2/(j+2-\omega)}$.

   (b) The shock speed (Eq. 16): $U = [2/(j+2-\omega)]\,(r_2/t)$.

   (c) The pre-shock density (Eq. 5): $\rho_1 = A\, r_2^{-\omega}$.

   (d) The immediate post-shock state (Eq. 13):
   $v_2 = [2/(\gamma+1)]\, U$, $\rho_2 = [(\gamma+1)/(\gamma-1)]\, \rho_1$, $p_2 = [2/(\gamma+1)]\, \rho_1\, U^2$.

   (e) The post-shock state in $0 \le r < r_2$ as follows.

      i. In the *standard* case, $r = 0$ corresponds to V_0 (Eq. 23), so for $V_0 \le V \le V_2$, evaluate:

      A. $r = r_2\, \lambda(V)$,

      B. $v = v_2\, f(V)$,

      C. $\rho = \rho_2\, g(V)$,

      D. $p = p_2\, h(V)$,

where $\lambda, \ldots, h$ are given in Eqs. 38–41.

ii. In the *singular* case, although V has the unique value V^* (Eq. 19), $r = 0$ corresponds to $\lambda = 0$ and $r = r_2$ corresponds to $\lambda = 1$, so for $0 \le \lambda \le 1$, evaluate (from Eqs. 88–92):

A. $r = r_2 \, \lambda$,

B. $v = v_2 \, \lambda$,

C. $\rho = \rho_2 \, \lambda^{j-2}$,

D. $p = p_2 \, \lambda^j$.

iii. In the *vacuum* case, $r = r_v$ corresponds to V_v (Eq. 28), so for $0 \le r \le r_v$ all quantities are zero, and for $V_2 \le V \le V_v$, evaluate:

A. $r = r_2 \, \lambda(V)$,

B. $v = v_2 \, f(V)$,

C. $\rho = \rho_2 \, g(V)$,

D. $p = p_2 \, h(V)$,

where $\lambda, \ldots, h$ are given in Eqs. 38–41.

4. The solution at a specific location $r = \tilde{r}$ can be obtained as follows:

   (a) In the standard and vacuum cases, identify the values of r (calculated in step 3(e)iA) that bracket $\tilde{r}$ and apply a root-finding routine (e.g., `zeroin` [25]) to obtain the corresponding value $\tilde{V}$, from which the entire state can be calculated according to steps B–D of 3(e)i or 3(e)iii.

   (b) In the singular case, solve for the value of λ at $r = \tilde{r}$ from Eq. 8, and obtain the remaining solution values from the relations given in steps B–D of 3(e)ii.

There are two sensitive computational issue in this procedure, both related to numerical quadrature of steps 2(a)i and ii in the standard and vacuum cases. First, since the lower limit of the integral is a singular limit of the integrands, it should be augmented by a small amount to evaluate the integral. Second, empirical evidence suggests that different adaptive quadrature routines provide slightly different answers in some circumstances. Anyone attempting to implement this procedure is advised to carefully evaluate the results of those numerical quadratures.

4 Results

In this section we present results for the constant initial density ($\omega = 0$) in §4.1 and for the power-law initial density ($\omega \neq 0$) in §4.2. Results of the closed-form solution are compared with results from the RAGE hydrocode [1] in §4.3.

4.1 Constant Initial Density Test Cases

The constant initial density case is that most frequently used in hydrocode verification tests, as the initial conditions are typically straightforward to prescribe in hydrocodes.

This case also admits verification by comparison of values of the similiarity variables λ, f, g, and h with the values published for $\gamma = 1.4$ in the tables in pp. 222-223 of Sedov's book [18]. Those published values appear to be tabulated using λ as the independent variable. Since the method we have outlined uses V as the independent variable, we obtain solutions at Sedov's tabulated values by first finding values of V corresponding to λs that bracket the published value of λ. Using the root finding routine `zeroin` [25], it is a straightforward task to calculate the value of V that corresponds to the desired λ value. In Tables 1, 2, and 3 we provide the numerical values from the tables in [18] (denoted "Sedov" in the tables) as well as the values calculated with the code based on the procedures outlined in this note (denoted "Exact"). Most of these values match exactly, i.e., to four significant figures; the majority of the remaining values match to three significant figures; a few match to only two significant figures. We speculate the following four reasons as causes of the disagreements: (i) the limited precision for λ provided in [18]), (ii) inexactness in the root-finding routine used to match the published value of λ; (iii) differences in the numerical quadrature routines used; and (iv) possible precision differences in the calculations.

The uniform density initial condition has been used for hydrocode comparison [3, 9, 13, 14, 17], primarily in spherical geometry. Although these authors set the undisturbed uniform density to unity, each uses a different initial energy source; i.e., in the literature for this problem, there does not appear to be a standard initial configuration, *à la* the Sod shock tube problem [20] or the Woodward-Colella blast wave problem [8]).

Therefore, we consider the following problems, based on that proposed by R. Klein and J. Bolstad [11] for spherical symmetry. Set the undisturbed uniform iniital density to $\rho_0 = 1$ g/cm^3 (i.e., $A = 1$ and $\omega = 0$) in a $\gamma = 1.4$ polytropic gas with initial energy $\mathcal{E}_0 = 0.0673185$, 0.311357, and 0.851072 ergs in the planar, cylindrical, and spherical cases, respectively. These values are chosen so that the shock is at $r = 0.5$, 0.75, and 1.0 in the planar, cylindrical, and spherical cases, respectively, at the chose time of $t = 1$ s. Compute the solution at the centers of 120 equally sized zones on the domain between the origin and 1.2, i.e., at $r_i = 0.005 + 0.01\,(i-1)$ cm, $i = 1, \ldots, 120$. Characteristics of the solutions for these problems are presented in Table 4. Figure 1 contains plots of the density, velocity, SIE, and pressure for these problems. These figures show the peak in the density and pressure immediately behind the shock, and the peak in SIE near the origin. In each case, the pressure asymptotes to a nonzero value at the origin; since the density vanishes there, the SIE grows without bound. The calculated shocks are sharp; the small smearing near the shock is an artifact of plotting the results at 100 points on the unit interval.

λ	V	Sedov f	Exact f	Sedov g	Exact g	Sedov h	Exact h
0.9797	0.5500	0.9699	0.9699	0.8625	0.8620	0.9162	0.9159
0.9420	0.5400	0.9156	0.9157	0.6659	0.6662	0.7915	0.7917
0.9013	0.5300	0.8599	0.8598	0.5160	0.5159	0.6923	0.6922
0.8565	0.5200	0.8017	0.8017	0.3982	0.3981	0.6120	0.6119
0.8050	0.5100	0.7390	0.7390	0.3019	0.3020	0.5457	0.5458
0.7419	0.5000	0.6678	0.6677	0.2200	0.2201	0.4904	0.4905
0.7029	0.4950	0.6263	0.6263	0.1823	0.1823	0.4661	0.4661
0.6553	0.4900	0.5780	0.5780	0.1453	0.1453	0.4437	0.4437
0.5925	0.4850	0.5172	0.5173	0.1074	0.1075	0.4229	0.4230
0.5396	0.4820	0.4682	0.4682	0.0826	0.0826	0.4116	0.4112
0.4912	0.4800	0.4244	0.4244	0.0641	0.0641	0.4038	0.4037
0.4589	0.4790	0.3957	0.3957	0.0536	0.0535	0.4001	0.4001
0.4161	0.4780	0.3580	0.3580	0.0415	0.0415	0.3964	0.3964
0.3480	0.4770	0.2988	0.2988	0.0263	0.0263	0.3929	0.3929
0.2810	0.4765	0.2410	0.2410	0.0153	0.0153	0.3911	0.3911
0.2320	0.4763	0.1989	0.1989	0.0095	0.0095	0.3905	0.3905
0.1680	0.4762	0.1441	0.1440	0.0042	0.0042	0.3901	0.3901
0.1040	0.4762	0.0891	0.0891	0.0013	0.0013	0.3900	0.3900

Table 1: Comparison of similarity variables for the $\gamma = 1.4$, planar geometry case. The Sedov values are those published in [18]. The exact values are those calculated with the present solution method. Values that differ are highlighted.

λ	V	Sedov f	Exact f	Sedov g	Exact g	Sedov h	Exact h
0.9998	0.4166	0.9996	0.9996	0.9973	0.9972	0.9985	0.9984
0.9802	0.4100	0.9645	0.9645	0.7653	0.7651	0.8659	0.8658
0.9644	0.4050	0.9374	0.9374	0.6285	0.6281	0.7832	0.7829
0.9476	0.4000	0.9097	0.9097	0.5164	0.5161	0.7124	0.7122
0.9295	0.3950	0.8812	0.8812	0.4234	0.4233	0.6514	0.6513
0.9096	0.3900	0.8514	0.8514	0.3451	0.3450	0.5983	0.5982
0.8725	0.3820	0.7998	0.7999	0.2427	0.2427	0.5266	0.5266
0.8442	0.3770	0.7638	0.7638	0.1892	0.1892	0.4884	0.4884
0.8094	0.3720	0.7226	0.7226	0.1414	0.1415	0.4545	0.4545
0.7629	0.3670	0.6720	0.6720	0.0975	0.0974	0.4242	0.4241
0.7242	0.3640	0.6327	0.6327	0.0718	0.0718	0.4074	0.4074
0.6894	0.3620	0.5989	0.5990	0.0545	0.0545	0.3969	0.3969
0.6390	0.3600	0.5521	0.5521	0.0362	0.0362	0.3867	0.3867
0.5745	0.3585	0.4943	0.4943	0.0208	0.0208	0.3794	0.3794
0.5180	0.3578	0.4448	0.4448	0.0123	0.0123	0.3760	0.3760
0.4748	0.3575	0.4073	0.4074	0.0079	0.0079	0.3746	0.3746
0.4222	0.3573	0.3621	0.3620	0.0044	0.0044	0.3737	0.3737
0.3654	0.3572	0.3133	0.3133	0.0021	0.0021	0.3733	0.3732
0.3000	0.3572	0.2571	0.2572	0.0008	0.0008	0.3730	0.3730
0.2500	0.3571	0.2143	0.2143	0.0003	0.0003	0.3729	0.3729
0.2000	0.3571	0.1714	0.1714	0.0001	0.0001	0.3729	0.3729
0.1500	0.3571	0.1286	0.1286	0.0000	0.0000	0.3729	0.3729
0.1000	0.3571	0.0857	0.0857	0.0000	0.0000	0.3729	0.3729

Table 2: Comparison of similarity variables for the $\gamma = 1.4$, cylindrical geometry case. The Sedov values are those published in [18]. The exact values are those calculated with the present solution method. Values that differ are highlighted.

λ	V	Sedov f	Exact f	Sedov g	Exact g	Sedov h	Exact h
0.9913	0.3300	0.9814	0.9814	0.8379	0.8388	0.9109	0.9116
0.9773	0.3250	0.9529	0.9529	0.6457	0.6454	0.7993	0.7992
0.9622	0.3200	0.9237	0.9238	0.4978	0.4984	0.7078	0.7082
0.9342	0.3120	0.8744	0.8745	0.3241	0.3248	0.5923	0.5929
0.9080	0.3060	0.8335	0.8335	0.2279	0.2275	0.5241	0.5238
0.8747	0.3000	0.7872	0.7872	0.1509	0.1508	0.4674	0.4674
0.8359	0.2950	0.7397	0.7398	0.0967	0.0968	0.4272	0.4273
0.7950	0.2915	0.6952	0.6952	0.0621	0.0620	0.4021	0.4021
0.7493	0.2890	0.6496	0.6497	0.0379	0.0379	0.3856	0.3857
0.6788	0.2870	0.5844	0.5844	0.0174	0.0174	0.3732	0.3732
0.5794	0.2860	0.4971	0.4971	0.0052	0.0052	0.3672	0.3672
0.4560	0.2857	0.3909	0.3909	0.0009	0.0009	0.3656	0.3656
0.3600	0.2857	0.3086	0.3086	0.0002	0.0001	0.3655	0.3655
0.2960	0.2857	0.2538	0.2537	0.0000	0.0000	0.3655	0.3655
0.2000	0.2857	0.1714	0.1714	0.0000	0.0000	0.3655	0.3655
0.1040	0.2857	0.0892	0.0891	0.0000	0.0000	0.3655	0.3655

Table 3: Comparison of similarity variables for the $\gamma = 1.4$, spherical geometry case. The Sedov values are those published in [18]. The exact values are those calculated with the present solution method. Values that differ are highlighted.

Geometry	$\mathcal{E}_0$	α	J_1	J_2
Planar	0.0673185	0.538548	0.197928	0.175834
Cylindrical	0.311357	0.984041	0.0654053	0.0495650
Spherical	0.851072	0.851060	0.0296269	0.0211647

Geometry	r_2	ρ_2	v_2	e_2	p_2
Planar	0.500000	6.00000	0.277778	0.0385802	0.0925926
Cylindrical	0.750000	6.00000	0.312500	0.0488281	0.117188
Spherical	1.00000	6.00000	0.333334	0.0555559	0.133334

Table 4: Comparison of variables for the $\gamma = 1.4$ uniform density test case at $t = 1$. The upper table contains the total energy $\mathcal{E}_0$, the nondimensional energy α (Eq. 66), and the integrals J_1 (Eq. 67) and J_2 (Eq. 68), while the lower table gives the the shock position r_2, and the post-shock density ρ_2, velocity v_2, SIE e_2, and pressure p_2.

4.2 Variable Initial Density Test Cases

The variable initial density case is less frequently used in hydrocode verification tests, as it is less straightforward to set up the initial conditions in codes; indeed, we have been unable to locate any hydrocode results using this problem in a refereed publication. We consider, therefore, two problems, the first of which is a singular case, and the second of which is a vacuum problem, the spherically symmetric version of which has been proposed by R. Klein and J. Bolstad [11].

For the singular problem we set $\gamma = 1.4$ and assign the initial density parameter to $A = 1$. Recall that there is no physically admissible singular solution in planar geometry. We set the density decay rate ω to be $5/3$ in the cylindrical case and $7/3$ in the spherical case, and vary the initial energy from approximately 2.46 in the cylindrical case to approximately 4.91 in the spherical case. The precise energy values are chosen so that the shock is at $r = 0.75$ in the cylindrical case and at $r = 1$ in the spherical case. As in the previous problems, the solution is computed at the center of 120 equally sized zones on the domain between the origin and 1.2. In Table 5 are presented various key values as computed for these cases. Figure 2 contains plots of the density, velocity, SIE, and pressure as functions of position for these two problems.

For the vacuum problem, we again consider a $\gamma = 1.4$ polytropic gas and set the initial density parameter to $A = 1$. As in the singular case, there is no physically admissible vacuum solution in planar geometry. We set the density decay rate ω to be 1.7 in the cylindrical case and 2.4 in the spherical case, and vary the initial energy from approximately 2.7 in the cylindrical case to approximately 5.5 in the spherical case. The spherical case is that proposed

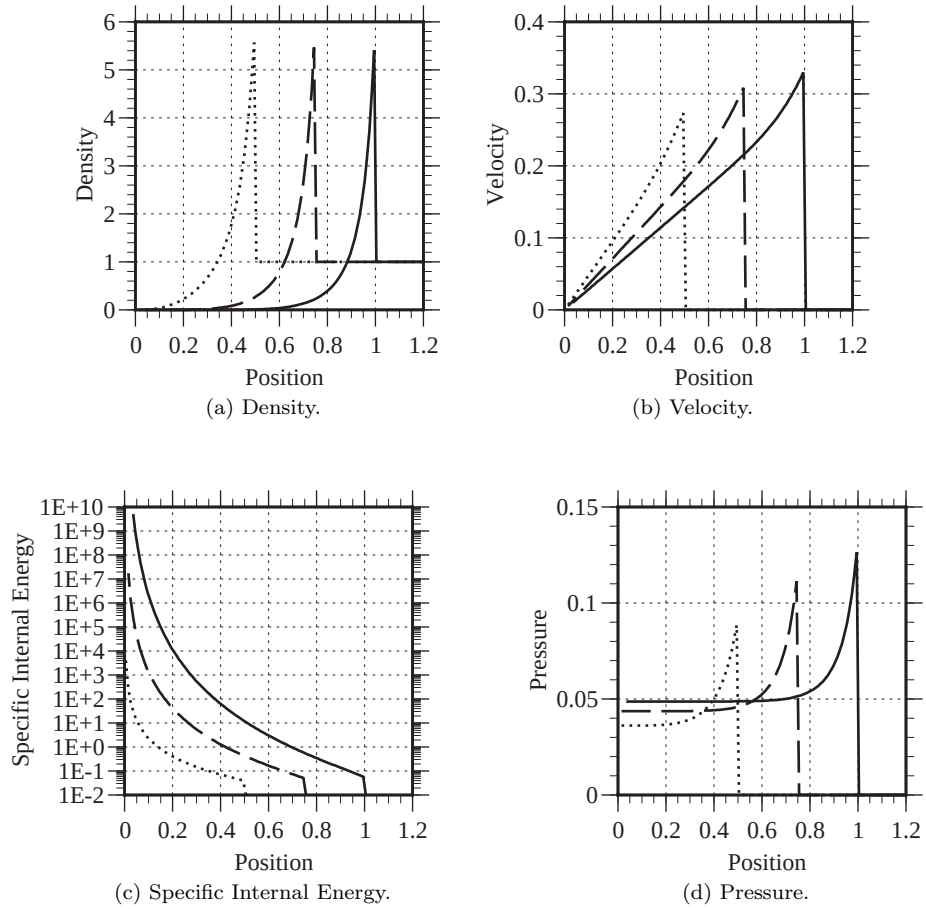

(a) Density. (b) Velocity.

(c) Specific Internal Energy. (d) Pressure.

Figure 1: Results of the $\gamma = 1.4$, uniform density test cases, corresponding to Table 4. Clockwise from the upper left are the density, velocity, pressure, and SIE for the planar (dotted), cylindrical (dashed), and spherical (solid) geometries, computed at 120 zones equally spaced on the domain [0,1.2].

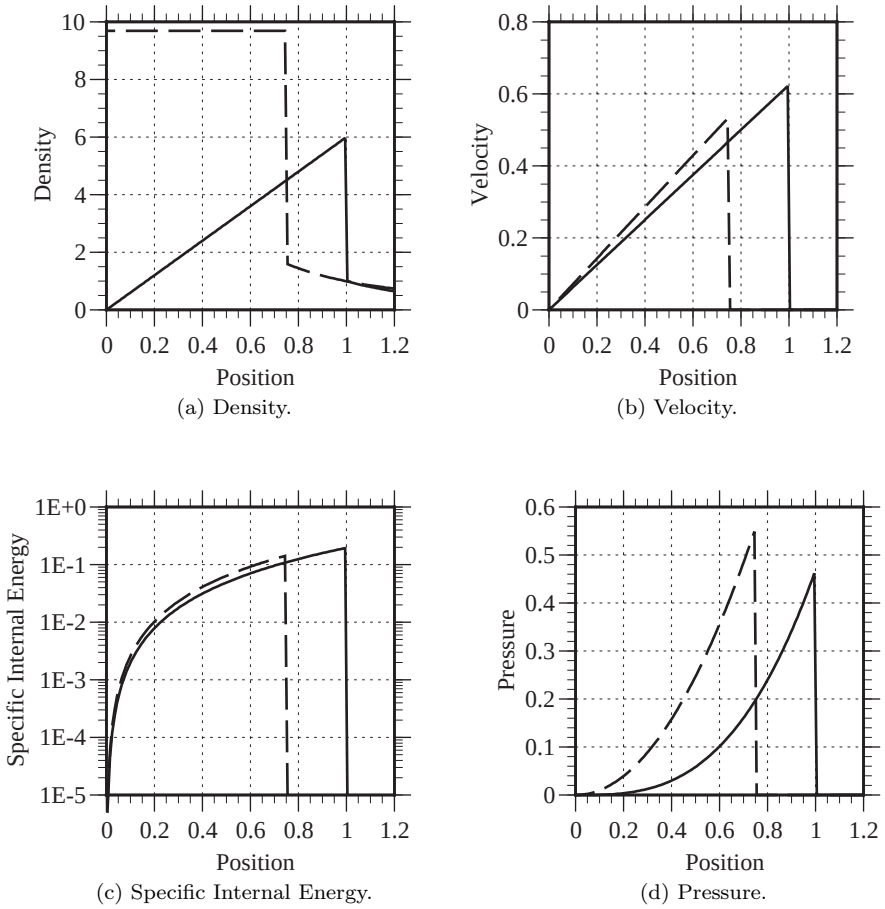

(a) Density. (b) Velocity.

(c) Specific Internal Energy. (d) Pressure.

Figure 2: Results of the $\gamma = 1.4$, singular test cases at $t = 1$, corresponding to Table 5. Clockwise from the upper left are the density, velocity, pressure, and SIE for the cylindrical (dashed) and spherical (solid) geometries, computed at 120 zones equally spaced on the domain [0,1.2].

Geometry	$\mathcal{E}_0$	ω	α
Cylindrical	2.45749	1.66667	4.80856
Spherical	4.90875	2.33333	4.90875

Geometry	r_2	ρ_2	v_2	e_2	p_2
Cylindrical	0.75	9.69131	0.535714	0.143495	0.556261
Spherical	1.00	6.00000	0.625000	0.195313	0.468750

Table 5: Comparison of variables for the $\gamma = 1.4$ singular test cases at $t = 1$. The upper table contains the total energy $\mathcal{E}_0$, the intial density exponent ω, and the nondimensional energy α (Eq. 66), while the lower table gives the the shock position r_2, and the post-shock density ρ_2, velocity v_2, SIE e_2, and pressure p_2.

by R. Klein and J. Bolstad [11] as a hydrocode verification problem. As in the previous problems, the solution is computed at the center of 120 equally sized zones on the domain between the origin and 1.2. In Table 6 are presented various key values as computed for these cases. Figure 3 contains plots of the density, velocity, SIE, and pressure as functions of position for these two problems.

4.3 Hydrocode Comparisons

In this section we compare the some of the test cases described above with results of the RAGE hydrocode [1]. In all cases, code results are for the 1D spherical symmetry only. We first examine the uniform initial density case of the previous section. We then consider two cases with radially varying initial density: one being the singular case of the previous section, and the other being the vacuum case of the previous section.

4.3.1 Uniform Density Problem Comparison

We calculated the 1D spherical test problem given in Table 4 with RAGE. The problem was on the domain $[0, 1.2]$, and run to a final time of $t = 1$. Graphical results of this case are given in Fig. 4 for 120 zones on $[0, 1.2]$ and Fig. 5 for 960 zones on $[0, 1.2]$. These figures show the density, velocity, SIE, and pressure from RAGE (dashed line) as well as the "exact" solution (solid line), plotted against the left axis, in addition to the absolute difference between these values (dotted line), plotted against the right axis.

The disagreement between the exact and hydrocode solutions is notable, particularly in the vicinity of the shock. We speculate that this error is largely due to the fact that in the hydrocode calculation, the initial energy is deposited

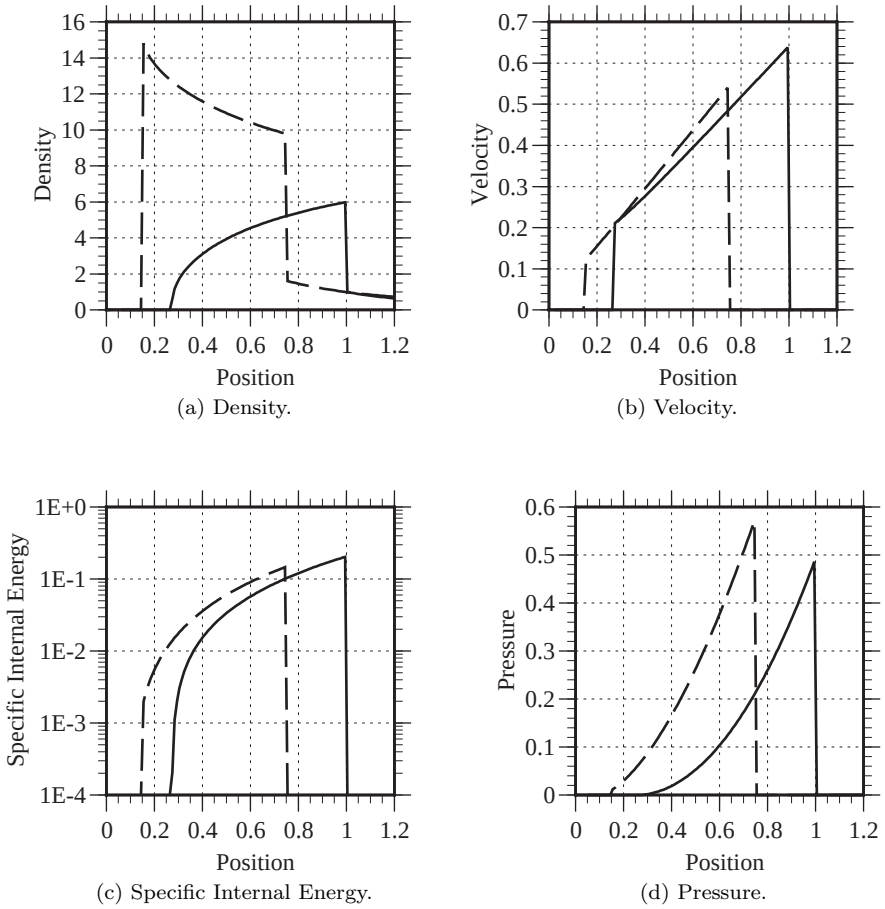

(a) Density. (b) Velocity.

(c) Specific Internal Energy. (d) Pressure.

Figure 3: Results of the $\gamma = 1.4$, vacuum test cases at $t = 1$, corresponding to Table 6. Clockwise from the upper left are the density, velocity, pressure, and SIE for the cylindrical (dashed) and spherical (solid) geometries, computed at 120 zones equally spaced on the domain [0,1.2].

Geometry	$\mathcal{E}_0$	ω	α	J_1	J_2
Cylindrical	2.67315	1.70	5.18062	0.856238	0.158561
Spherical	5.45670	2.40	5.45670	0.454265	0.0828391

Geometry	r_v	r_2	ρ_2	v_2	e_2	p_2
Cylindrical	0.154090	0.750000	9.78469	0.543478	0.147684	0.578018
Spherical	0.272644	1.00000	6.00000	0.641026	0.205457	0.493097

Table 6: Comparison of variables for the $\gamma = 1.4$ vacuum test cases at $t = 1$. The upper table contains the total energy $\mathcal{E}_0$, the intial density exponent ω, the nondimensional energy α (Eq. 66), and the integrals J_1 (Eq. 67) and J_2 (Eq. 68), while the lower table gives the vacuum boundary position r_v, shock position r_2, and the post-shock density ρ_2, velocity v_2, SIE e_2, and pressure p_2.

in the zone nearest the origin; that is, it is not a true delta-function initial condition. We surmise that the finite nature of the hydrocode initial condition imprints on the subsequent dynamics, leading to values that differ somewhat from those of the exact solution.

Comparison of these two figures gives some notion of the convergence of the calculation under grid refinement. This concept is rigorously quantified in Table 7, which gives asymptotic spatial convergence rates[1] for RAGE calculations with 120-240-480 zones and 240-480-960 zones. We include four convergence rates: mean, L_1, L_2, L_∞; typically, the L_1 convergence rate is used for problems with shocks. For these variables, all convergence rates are sublinear; indeed, the SIE convergence rates appear anomalous. From these results, it is clear that the calculation is converging.

[1]See Appendix A for a discussion of convergence rates and how they are calculated.

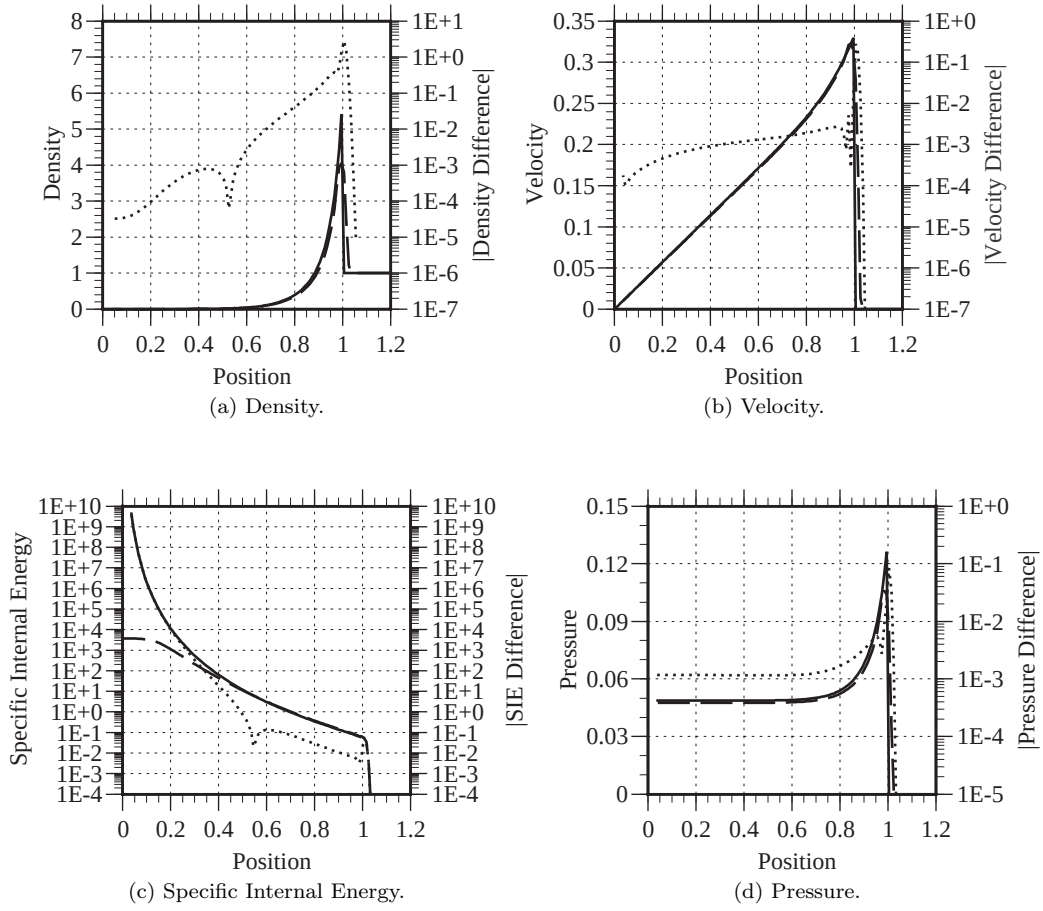

(a) Density.

(b) Velocity.

(c) Specific Internal Energy.

(d) Pressure.

Figure 4: Results of RAGE on the 1D, spherical, $\gamma = 1.4$, uniform density test case with total energy $\mathcal{E}_0 = 0.851072$, corresponding to Table 4. Clockwise from the upper left are the density, velocity, pressure, and SIE for RAGE (dashed) and the exact (solid) solutions, both plotted against the left axis, as well as the absolute difference (dotted), plotted against the right axis. Both solutions were calculated at the centers of 120 zones equally spaced on the domain $[0, 1.2]$.

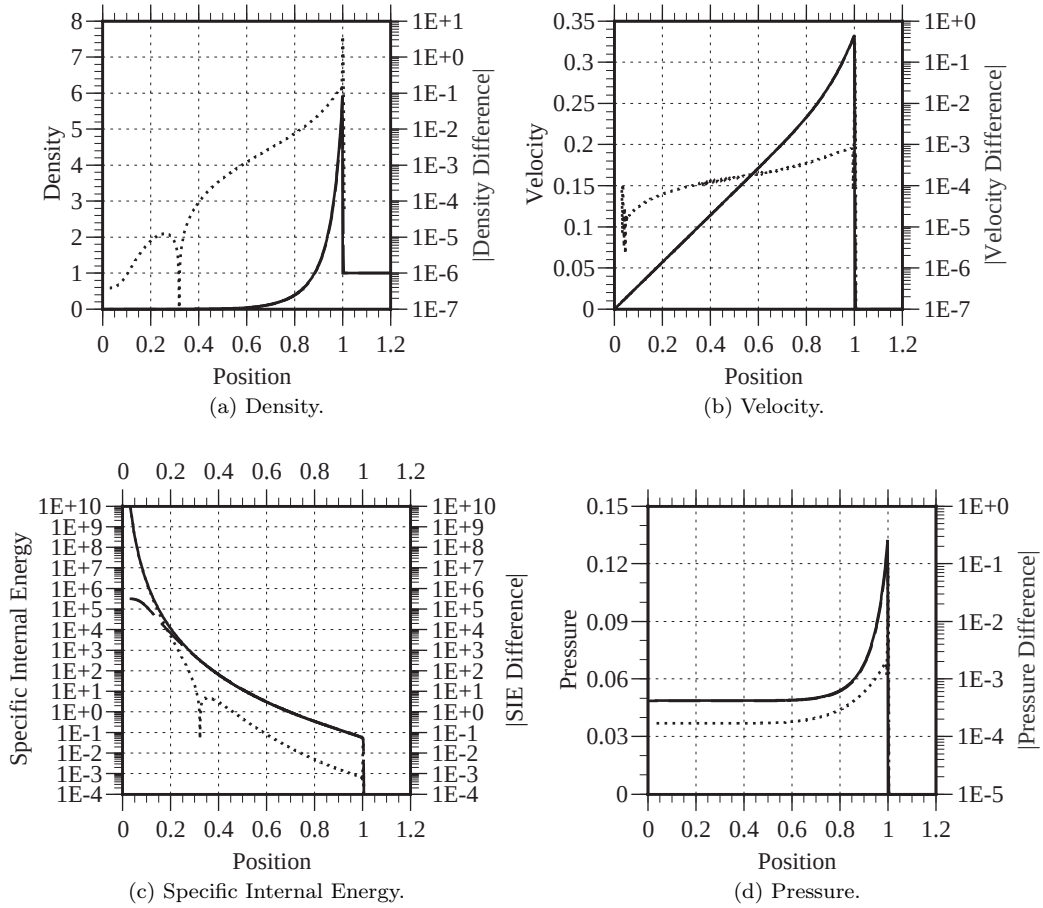

(a) Density.

(b) Velocity.

(c) Specific Internal Energy.

(d) Pressure.

Figure 5: Results of RAGE on the 1D, spherical, $\gamma = 1.4$, uniform density test case with total energy $\mathcal{E}_0 = 0.851072$, corresponding to Table 4. Clockwise from the upper left are the density, velocity, pressure, and SIE for RAGE (dashed) and the exact (solid) solutions, both plotted against the left axis, as well as the absolute difference (dotted), plotted against the right axis. Both solutions were calculated at the centers of 960 zones equally spaced on the domain $[0, 1.2]$.

Density Convergence Rates

	100–200–400	200–400–800
$\hat{n}$	0.7418	0.4502
n_{L_1}	0.5937	0.7191
n_{L_2}	0.4445	0.4973
n_{L_∞}	0.3765	0.4242

Pressure Convergence Rates

	100–200–400	200–400–800
$\hat{n}$	0.8836	0.8389
n_{L_1}	0.7666	0.7687
n_{L_2}	0.3338	0.4309
n_{L_∞}	0.1527	0.3154

SIE Convergence Rates

	100–200–400	200–400–800
$\hat{n}$	0.06813	0.2039
n_{L_1}	-1.857	-1.857
n_{L_2}	-2.001	-2.000
n_{L_∞}	-2.145	-2.144

Velocity Convergence Rates

	100–200–400	200–400–800
$\hat{n}$	0.9983	0.8017
n_{L_1}	0.8208	0.8269
n_{L_2}	0.5653	0.6630
n_{L_∞}	0.5267	0.6471

Table 7: Asymptotic spatial convergence rates for RAGE calculations of the uniform-density Sedov test problem. For each of the sets of calculations, where the column headings correspond to the number of zones on $[0, 1]$, listed are the mean pointwise, L_1, L_2, and L_∞ convergence rates at $t = 1$ for, from top to bottom, density, pressure, SIE, and velocity. See Appendix A for a discussion of convergence rates.

4.3.2 Singular Problem Comparison

We next consider the 1D spherical singular test problem described in Table 5, with results previously shown in Fig. 2. The problem is on the domain $[0, 1.2]$, and run to a final time of $t = 1$. Graphical results of this case are given in Fig. 6 for 120 zones on $[0, 1.2]$ and Fig. 7 for 960 zones on $[0, 1.2]$. These figures show the density, velocity, SIE, and pressure from RAGE (dashed line) as well as the "exact" solution (solid line), plotted against the left axis, in addition to the absolute difference between these values (dotted line), plotted against the right axis.

The code results exhibit singificant errors in the region near the origin, which, in this case, should have linearly vanishing density and velocity as the origin is approached. Examination of results at earlier times suggest an inability of the hydrodynamics algorithm to move the initial high density, high energy material out of the near-origin zone; this incorrect mass distribution leading to a series of reflected and converging waves that pollute the solution at later time. Comparison of Figs. 6 and 7, however, suggests improvement, albeit slow, under mesh refinement, particularly adjacent to the shock. Additionally, all quantities decrease by approximately a factor of two with the eightfold increase in zoning in the vicinity of the origin. Less extensive testing of other hydrocodes [12, 15], both Eulerian and Lagrangian, on this problem revealed similar difficulties.

Calculated asymptotic convergence rates for this problem are provided in Table 8. RAGE calculations with 120-240-480 zones and 240-480-960 zones on $[0, 1.2]$ were used in those calculations. Those results suggest that the 120-240-480 zone calculations are not within the domain of asymptotic convergence, while the 240-480-960 zone set may be. It is unclear from those convergence rate values if the code results are approaching the exact solution.

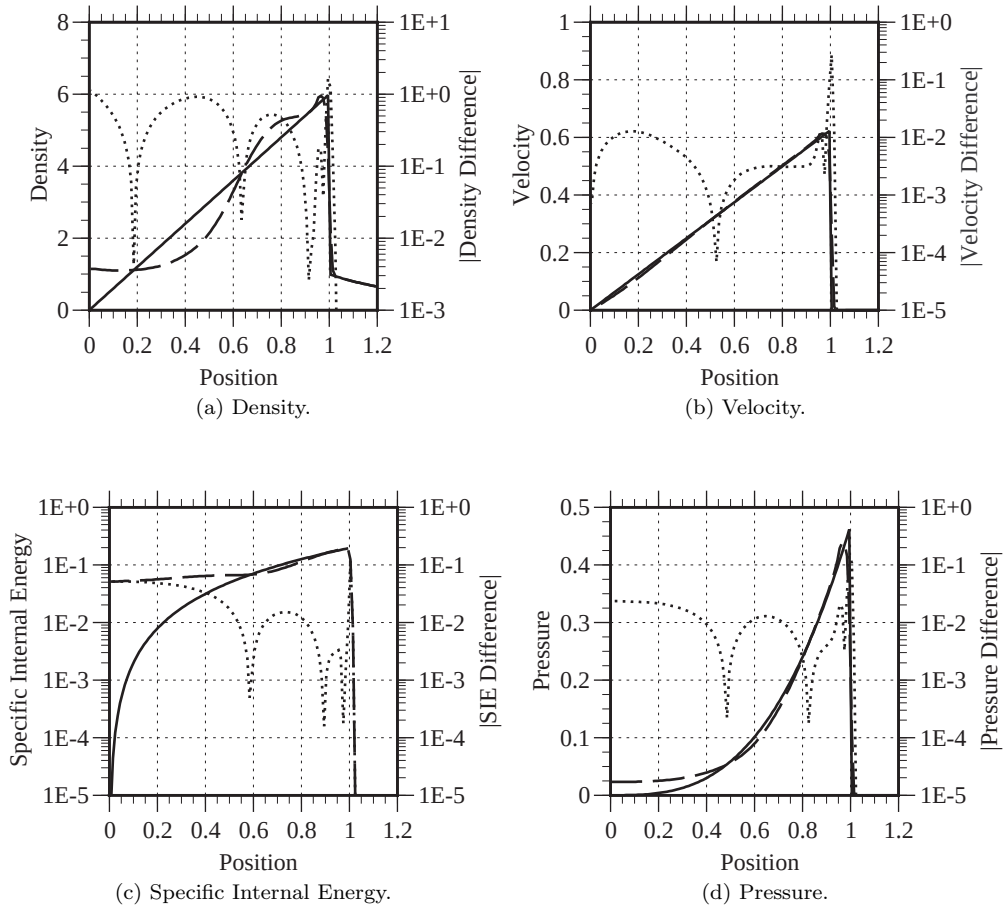

(a) Density. (b) Velocity.

(c) Specific Internal Energy. (d) Pressure.

Figure 6: Results of RAGE on the 1D, spherical, $\gamma = 1.4$, singular test case with total energy $\mathcal{E}_0 = 5.45670$ and initial density $\rho_0(r) = r^{-2.4}$, corresponding to Table 6. Clockwise from the upper left are the density, velocity, pressure, and SIE for RAGE (dashed) and the exact (solid) solutions, both plotted against the left axis, as well as the absolute difference (dotted), plotted against the right axis. Both solutions were calculated at the centers of 120 zones equally spaced on the domain $[0, 1.2]$.

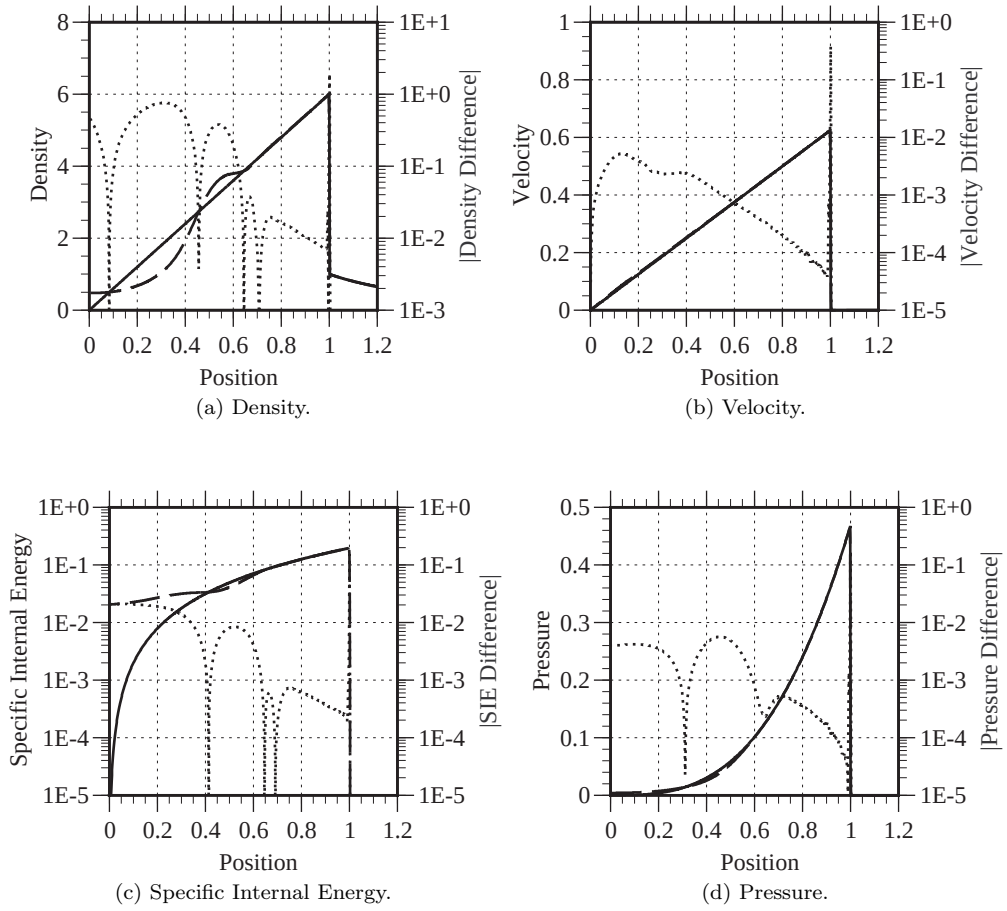

(a) Density.

(b) Velocity.

(c) Specific Internal Energy.

(d) Pressure.

Figure 7: Results of RAGE on the 1D, spherical, $\gamma = 1.4$, singular test case with total energy $\mathcal{E}_0 = 5.45670$ and initial density $\rho_0(r) = r^{-2.4}$, corresponding to Table 6. Clockwise from the upper left are the density, velocity, pressure, and SIE for RAGE (dashed) and the exact (solid) solutions, both plotted against the left axis, as well as the absolute difference (dotted), plotted against the right axis. Both solutions were calculated at the centers of 960 zones equally spaced on the domain $[0, 1.2]$.

Density Convergence Rates

	100–200–400	200–400–800
$\hat{n}$	-0.07694	0.6900
n_{L_1}	-0.06701	0.5189
n_{L_2}	-0.01540	0.3732
n_{L_∞}	0.7123	0.2035

Pressure Convergence Rates

	100–200–400	200–400–800
$\hat{n}$	0.8416	1.052
n_{L_1}	0.4893	1.018
n_{L_2}	0.4713	0.7224
n_{L_∞}	0.8318	0.4668

SIE Convergence Rates

	100–200–400	200–400–800
$\hat{n}$	0.3060	0.3862
n_{L_1}	0.3483	0.6141
n_{L_2}	0.2216	0.5260
n_{L_∞}	-0.03705	0.3919

Velocity Convergence Rates

	100–200–400	200–400–800
$\hat{n}$	2.278	0.9676
n_{L_1}	1.999	-0.5057
n_{L_2}	0.6335	0.2806
n_{L_∞}	-0.3283	0.4418

Table 8: Asymptotic spatial convergence rates for RAGE calculations of the Sedov singular problem. For each of the sets of calculations, where the column headings correspond to the number of zones on $[0, 1]$, listed are the mean pointwise, L_1, L_2, and L_∞ convergence rates at $t = 1$ for, from top to bottom, density, pressure, SIE, and velocity. See Appendix A for a discussion of convergence rates.

4.3.3 Vacuum Problem Comparison

Lastly, we consider the 1D spherical vacuum problem given in Table 6 and shown in Fig. 3. The problem was on the domain $[0, 1.2]$, and run to a final time of $t = 1$. Graphical results of this case are given in Fig. 8 for 120 zones on $[0, 1.2]$ and Fig. 9 for 960 zones on $[0, 1.2]$. These figures show the density, velocity, SIE, and pressure from RAGE (dashed line) as well as the "exact" solution (solid line), plotted against the left axis, in addition to the absolute difference between these values (dotted line), plotted against the right axis.

These results exhibit behavior similar to that of the singular case, namely, the inability to resolve the region near the origin, which, in this case should have vanishingly small density. Indeed, the entire vacuum region is poorly resolved in all of these calculations. As in the previous case, comparison of Figs. 8 and 9, however, shows improvement under mesh refinement, particularly near the shock. Improvement is also seen in the vacuum region, where, e.g., the error in both the density and pressure decreases by $\sim$50% with the eightfold increase in zones. Closer analysis of these calculations shows the same phenomenon as in the singular case, viz., the inability of the hydrodynamics algorithms to move the initial high density, high energy material out of the near-origin zone early in the calculation. This is the same pathological initial-condition imprinting as in the singular case. Less extensive testing of other hydrocodes [4, 12, 15], both Eulerian and Lagrangian, on this problem revealed similar difficulties.

Calculated asymptotic convergence rates for this problem are provided in Table 9. As in the singular case, these results suggest that the 120-240-480 zone calculations are not within the domain of asymptotic convergence, while the 240-480-960 zone set may be; the low convergence rates for density in that case suggest that it is not the case for that variable. It is unclear from those convergence rate values if the code results are approaching the exact solution in the vicinity of the vacuum region (in general) and the origin (in particular).

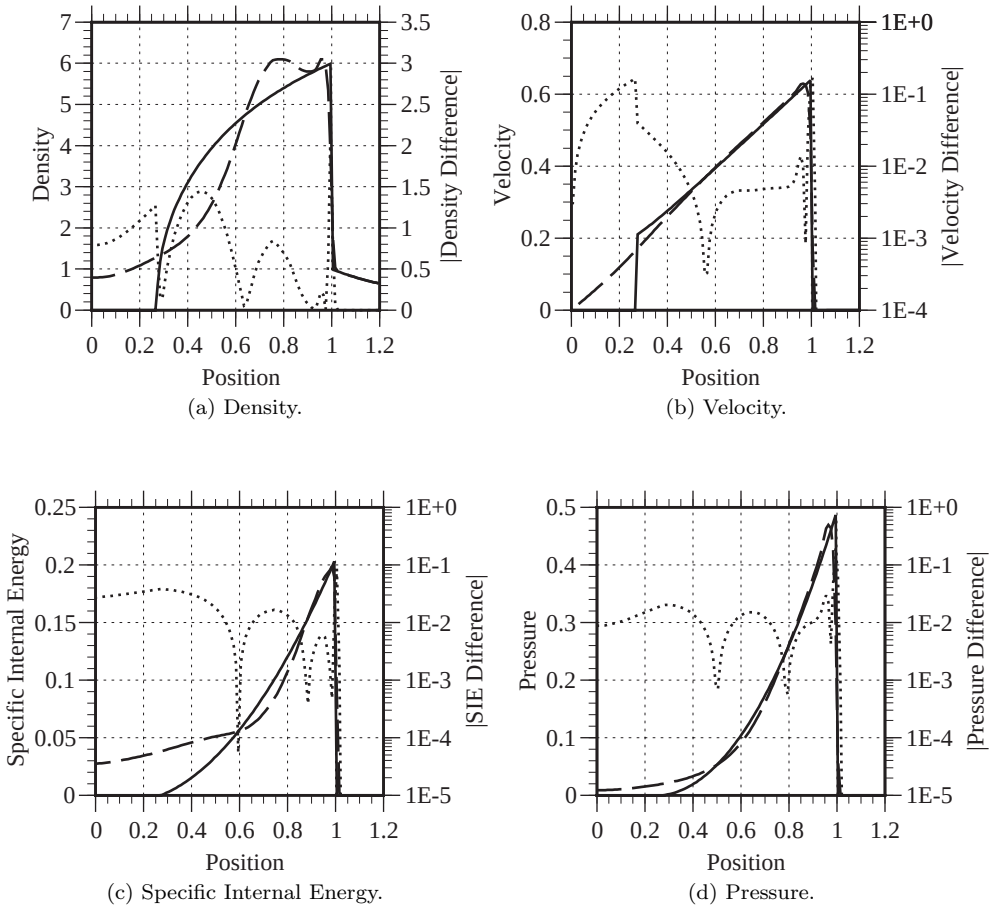

(a) Density.

(b) Velocity.

(c) Specific Internal Energy.

(d) Pressure.

Figure 8: Results of RAGE on the 1D, spherical, $\gamma = 1.4$, vacuum test case with total energy $\mathcal{E}_0 = 5.45670$ and initial density $\rho_0(r) = r^{-2.4}$, corresponding to Table 6. Clockwise from the upper left are the density, velocity, pressure, and SIE for RAGE (dashed) and the exact (solid) solutions, both plotted against the left axis, as well as the absolute difference (dotted), plotted against the right axis. Both solutions were calculated at the centers of 120 zones equally spaced on the domain $[0, 1.2]$.

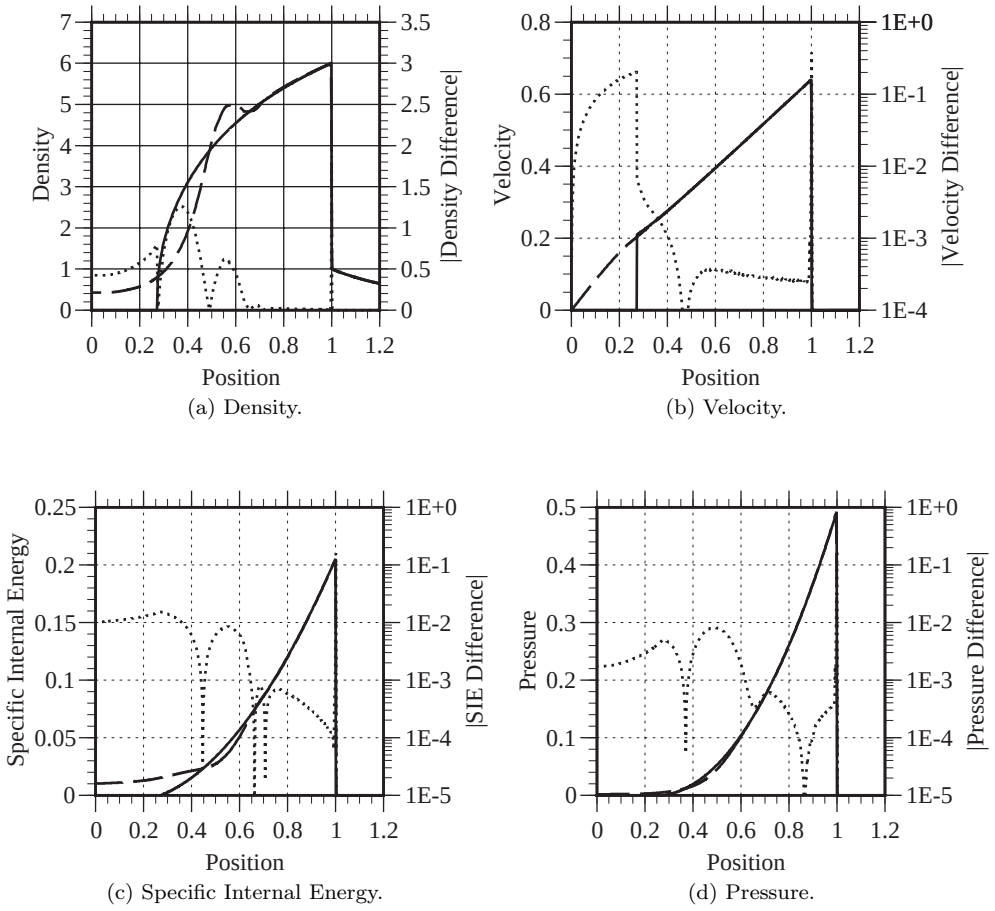

(a) Density.

(b) Velocity.

(c) Specific Internal Energy.

(d) Pressure.

Figure 9: Results of RAGE on the 1D, spherical, $\gamma = 1.4$, vacuum test case with total energy $\mathcal{E}_0 = 5.45670$ and initial density $\rho_0(r) = r^{-2.4}$, corresponding to Table 6. Clockwise from the upper left are the density, velocity, pressure, and SIE for RAGE (dashed) and the exact (solid) solutions, both plotted against the left axis, as well as the absolute difference (dotted), plotted against the right axis. Both solutions were calculated at the centers of 960 zones equally spaced on the domain $[0, 1.2]$.

Density Convergence Rates

	100–200–400	200–400–800
$\hat{n}$	-0.08326	0.2131
n_{L_1}	-0.03525	0.1283
n_{L_2}	0.05707	0.08358
n_{L_∞}	0.6052	0.05947

Pressure Convergence Rates

	100–200–400	200–400–800
$\hat{n}$	0.3482	1.083
n_{L_1}	0.5212	0.8079
n_{L_2}	0.8615	0.6551
n_{L_∞}	0.9804	0.5647

SIE Convergence Rates

	100–200–400	200–400–800
$\hat{n}$	0.4526	0.4567
n_{L_1}	0.3373	0.5270
n_{L_2}	0.2298	0.4519
n_{L_∞}	-0.8449	0.5123

Velocity Convergence Rates

	100–200–400	200–400–800
$\hat{n}$	0.4771	1.546
n_{L_1}	0.04443	1.416
n_{L_2}	0.01945	0.8952
n_{L_∞}	0.4351	0.4692

Table 9: Asymptotic spatial convergence rates for RAGE calculations of the Sedov vacuum problem. For each of the sets of calculations, where the column headings correspond to the number of zones on $[0, 1]$, listed are the mean pointwise, L_1, L_2, and L_∞ convergence rates at $t = 1$ for, from top to bottom, density, pressure, SIE, and velocity. See Appendix A for a discussion of convergence rates.

5 Summary

We have reviewed Sedov's solution, given in [18], for the problem of self-similar, one-dimensional, compressible hydrodynamics in which a finite amount of energy is released at the origin at the initial time. The main result of this report is given in §3, where we outline an algorithmic procedure for evaluating this solution, in terms of quantities and equations found primarily in §2, which contains an elaboration of Sedov's solution. In addition to the "standard Sedov problem," we have included the solution to the singular and vacuum problems in both cylindrical and spherical geometries.

In §4 we showed examples of these solutions. Such problems can be used in the verification of hydrodynamics codes. Computed asymptotic convergence rates based on hydrocode calculations of these problems showed sublinear convergence at best; calculations of the singular and vacuum did not converge on the coarsest grids (100-200-400 zones on the unit interval). We also compared hydrocode calculations with the exact solutions. Those comparisons suggest that the Godunov-type high-resolution method used in the RAGE hydrocode performs adequately on the standard Sedov problem, but may perform inadequately on problems for which the pressure vanishes at the origin. Although we have presented only RAGE results herein, less extensive testing of other hydrocodes [4, 12, 15], both Eulerian and Lagrangian, revealed similar difficulties for problems in which the pressure vanishes at and near the origin. Although the magnitude of the error in the vicinity of the origin diminishes under mesh refinement, we make the heuristic albeit plausible speculation that the hydrocode solution may not be not converging to the exact solution for these problems. We speculate that a possible fundamental shortcoming of present hydrodynamic integration methods for these highly singular flows may be uncovered by a thorough investigation of the singular and vacuum Sedov problems.

Acknowledgments

The careful reviews by Rob Lowrie and Bill Rider are kindly acknowledged. This work was performed by Los Alamos National Laboratory, which is operated by the University of California for the U.S. Department of Energy under contract W-7405-ENG-36.

References

[1] R. M. Baltrusaitis, M. L. Gittings, R. P. Weaver, R. P. Benjamin & J. M. Budzinski, Simulation of shock-generated instabilities, *Phys. Fluids* **8**(9), pp. 2471–2483 (1996).

[2] J. Bolstad, LLNL, personal communication.

[3] J.R. Buchler, Z. Kolláth & A. Marom, An Adaptive Code for Radial Stellar Model Pulsations, *Astrophys. Space Sci.* **253**, pp. 139–160 (1997).

[4] M. Clover, LANL, personal communication.

[5] S.V. Coggeshall, "Group-invariant Solutions of Hydrodynamics", in *Computational Fluid Dynamics: Selected Topics*, K.G. Roesner, D. Leutloff & R.C. Srivastava, eds., Springer, New York pp. 71–101 (1995).

[6] S.V. Coggeshall & R.A. Axford, Lie group invariance properties of radiation hydrodynamics equations and their associated similarity solutions, *Phys. Fluids* **29**(8), pp. 2398–2420 (1986).

[7] S.V. Coggeshall & J. Meyer-ter-Vehn, Group-invariant solutions of and optimal systems for multidimensional hydrodynamics, *J. Math. Phys.* **31**(10), pp. 3585–3601 (1992).

[8] P. Colella & P. R. Woodward, The Piecewise Parabolic Method (PPM) for Gas-dynamical Simulations, *J. Comp. Phys.* **54**, pp. 174–201 (1984).

[9] B. Fryxell, K. Olson, P. Ricker, R.X. Timmes, M. Zingale, D.Q. Lamb, P. MacNeice, R. Rosner, J.W. Truran & H. Tufo, FLASH: An Adaptive Mesh Hydrodynamics Code for Modeling Astrophysical Thermonuclear Flashes, *Astrophys. J. Suppl. Ser.* **131**, pp. 273–334 (2000).

[10] J. R. Kamm & W. J. Rider, *2-D Convergence Analysis of the RAGE Hydrocode*, Los Alamos National Laboratory Report LA-UR-98-3872 (1998).

[11] R. Klein & J. Bolstad, LLNL, personal communication.

[12] R. Lowrie, LANL, personal communication.

[13] J.M. Owen, J.V. Villumsen, P.R. Shapiro & H. Martel, Adaptive Smoothed Particle Hydrodynamics: Methodology. II., *Astrophys. J. Supp. Ser.* **116**, pp. 155–209 (1998).

[14] C. Reile & T. Gehren, Numerical simulation of photospheric convection in solar-type stars I. Hydrodynamical test calculations, *Astron. Astrophys.* **242**, pp. 142–174 (1991).

[15] W. Rider, LANL, personal communication.

[16] R. Reinicke & J. Meyer-ter-Vehn, The point explosion with heat conduction, *Phys. Fluids A* **3**(7), pp. 1807–1818 (1991).

[17] M. Shashkov & B. Wendroff, A Composite Scheme for Gas Dynamics in Lagrangian Coordinates, *J. Comp. Phys.* **150**, pp. 502–517 (1999).

[18] L.I. Sedov, *Similarity and Dimensional Methods in Mechanics*, Academic Press, New York, NY, p. 147 ff. (1959).

[19] A.I. Shestakov, Time-dependent simulations of point explosions with heat conduction, *Phys. Fluids* **11**(5), pp. 1091-1095 (1999).

[20] G. Sod, A survey of several finite difference methods for systems of nonlinear hyperbolic conservation laws, *J. Comp. Phys.* **27**, pp. 1–31 (1978).

[21] G.I. Taylor, The formation of a blast wave by a very intense explosion, *Proc. Roy. Soc. London A* **201**, pp. 159-174 (1950).

[22] H.A Bethe, K. Fuchs, J.O. Hirschfelder, J.L. Magee, R.E. Peierls, J. von Neumann, *Blast Wave*, Los Alamos Scientific Laboratory Report LA-2000, August 1947.

[23] G.B. Whitham, *Linear and Nonlinear Waves*, John Wiley & Sons, New York, NY, p. 177 (1974).

[24] The quadrature routines in ACM agorithm 691 are available from `Netlib` at `http://www.netlib.org/`.

[25] The `zeroin` routine is availabe from `Netlib` at `http://www.netlib.org/`.

A Spatial Convergence Analysis

For any variable ξ computed at a given uniform grid spacing Δx, the fundamental *Ansatz* of convergence analysis is that the difference between the exact and computed solutions can be expanded as a polynomial function of the grid spacing:

$$\xi^* - \xi_i = \mathcal{A}\ (\Delta x_i)^\tau + o\Big((\Delta x_i)^n\Big)\,, \tag{A1}$$

where ξ^* is the *exact* value, ξ_i is the value computed on the grid of spacing Δx_i, $\mathcal{A}$ is the *convergence coefficient*, and τ is the *convergence rate*. Using the solution on three different grids, related by a uniform mesh ratios, one obtains

$$\begin{aligned} \tau &= \frac{\log\left[\left(\xi_m - \xi_c\right) / \left(\xi_f - \xi_m\right)\right]}{\log \varsigma}\,, \\ \mathcal{A} &= -\frac{\xi_f - 2\xi_m + \xi_c}{(\Delta x)^\tau\ \left(\varsigma^{-\tau} - 1\right)^2}\,, \end{aligned} \tag{A2}$$

where the subscripts c, m, and f refer to the coarse-, medium-, and fine-grid solutions, respectively, and ς is the uniform ratio of the medium-to-coarse grids and fine-to-medium grids. To apply these results computationally, the data on the medium and fine grids must be averaged onto the coarse grid. Typically, the ratio of grid sizes is taken to be two, and the following procedure is applied: the volume-weighted means of the two bracketing values of the medium solution and the four bracketing values of the fine solution are calculated and used as the cell-averaged values at the corresponding coarse gridpoint. For example, using density as the variable of interest and assuming the coarse grid has N points, values $\rho^m_{i'}$ from the i'th zone (which has volume $V^m_{i'}$) of the medium-grid solution, $i' = 1, \ldots, 2N$, are interpolated to the value $\rho_i^{c\leftarrow m}$ at locations x_i, $i = 1, \ldots, N$, on the coarse grid as

$$\rho_i^{c\leftarrow m} = \left(V^m_{2i-1}\rho^m_{2i-1} + V^m_{2i}\rho^m_{2i}\right) / \left(V^m_{2i-1} + V^m_{2i}\right)\ . \tag{A3}$$

Similarly, values from the fine solution, $\rho^f_{\hat{\imath}}$, $\hat{\imath} = 1, \ldots, 4N$, are interpolated to the locations $\rho_i^{c\leftarrow f}$ at the corresponding position on the coarse grid as

$$\rho_i^{c\leftarrow f} = \frac{V^f_{4i-3}\rho^f_{4i-3} + V^f_{4i-2}\rho^f_{4i-2} + V^f_{4i-1}\rho^f_{4i-1} + V^f_{4i}\rho^f_{4i}}{V^f_{4i-3} + V^f_{4i-2} + V^f_{4i-1} + V^f_{4i}}\,. \tag{A4}$$

These values are used in Eq. A2 to determine the pointwise convergence characteristics.

With the pointwise convergence rates, a mean convergence rate over the entire domain is constructed by taking the arithmetic average of the (local) convergence rate at each gridpoint, i.e.,

$$\hat{\tau} = \frac{1}{\hat{N}}\ \sum_i \tau_i\,, \tag{A5}$$

where τ_i is the asymptotic convergence rate computed at gridpoint x_i, $i = 1, \ldots, \hat{N}$. We indicate the total number of points in this average as $\hat{N}$ *not* as N, for the reason that all points on the computational grid might not be used in the evaluation of the mean pointwise convergence rate. For example, if the numerical values of the cell-averaged quantities from the fine and medium meshes are identical, then the expression for τ in Eq. A2 either diverges (if those values do not equal the value on the coarse mesh) or is undefined (if all values are identical). Similarly, the computed value of the argument of the logarithm in the numerator of Eq. A2 could be negative, leading to an imaginary value for τ. We include only well-defined pointwise convergence rates in Eq. A5 and find that, in general, $\hat{N} \neq N$.

The asymptotic convergence rate can also be computed with a global quantity. For example, the convergence rate for the norm of a computed quantity over the entire grid is given as

$$\tau \doteq \frac{\log\left[||\xi_m - \xi_c||/||\xi_f - \xi_m||\right]}{\log \varsigma}\,, \tag{A6}$$

where $||\cdot||$ denotes any consistent norm. For the global rates, we compute the L_1, L_2, and L_∞ norms in Eq. A6; using density as the variable of interest and the difference between values on the medium and coarse grids, these norms are defined as

$$||\rho^m - \rho^c||_1 \equiv \frac{1}{N}\sum_i \left|\rho_i^m - \rho_i^c\right|, \tag{A7}$$

$$||\rho^m - \rho^c||_2 \equiv \sqrt{\frac{1}{N}\sum_i \left|\rho_i^m - \rho_i^c\right|^2}\,, \tag{A8}$$

$$||\rho^m - \rho^c||_\infty \equiv \max_i\left\{\left|\rho_i^m - \rho_i^c\right|\right\}, \tag{A9}$$

where N is the number of gridpoints, and ρ_i^m and ρ_i^c are the density at x_i computed on the medium grid (interpolated to the coarse grid) and coarse grids, respectively. For the global convergence rate based on norms, *all* of the points in the domain of interest are perforce included in the evaluation of the norms, and, therefore, in the evaluation of the convergence rate. It is possible (though unlikely) that one or both of the norms in the numerator of the RHS of Eq. A6 could equal zero; in such a case, the convergence rate is undefined.